

The Earthquake Dissipative Engine: Energy Budget and Partition PART C: Dissipation



S. Nielsen

Short course on earthquake physics

Geoscienze, Università di Padova Oct 2025

27 Oct. - 16:30-18:30 classroom 2G

28 Oct. - 14:30-16:30 classroom 2H

29 Oct. - 10:30-12:30 classroom Lab Paleo

31 Oct. - 14:30-16:30 classroom 2L

1 The dissipation

This is not my fault _(シ)_/ : friction in every day's life

- Dry frictional contact
- Asperities
- Friction coefficient and linear normal stress dependence

It's been known since the times of Da Vinci, Amonton and Coulomb that frictional resistance to slip is proportional to normal load. A parallel can be made for rock friction as shown by Byerlee. Faults are quite different objects from every day's life engineering or household objects undergoing friction. However parallels can be made, and important concepts on friction have been cross-fertilizing between different disciplines.

A few points:

(a) The average spacing between the two rough surfaces does not vary significantly with normal load. Hertzian contact between two isolated, elastic spheres yields an interpenetration distance h varying non-linearly with the normal load in the form $h \propto F^{2/3}$. However, as shown in (Greenwood and Williamson 1966) and (Persson 2000), assuming that the surface topography of two solids in frictional contact across an area A can be mimicked by adjoining N spherical caps with average radius λ and a given probability distribution of height $\psi(z)$, the separation ω between two rough surfaces under a normal load F follows the equation:

$$\left(\frac{\omega}{\omega_0}\right)^2 = 2 \log \left(N \omega_0^{3/2} \lambda^{1/2} \frac{4}{3(1-v_P^2)} \frac{E}{F} \right) - 5 \log \left(\frac{\omega}{\omega_0} \right) \quad (1)$$

where ω_0 is the characteristic elevation of the asperities on the surface, e.g., the root mean square (rms) of the asperity height probability distribution $\psi(z)$ (z being the asperity height with respect to the reference plane $z = 0$ such that $\int_A \psi(z) da = 0$), ν_P is the Poisson ratio and E is the Young modulus of the medium. A schematic illustration of the meaning of the ω , ω_0 and λ in the above equation is provided in (Fig. 1).

Rough surfaces and fault veins: a mathematical frame

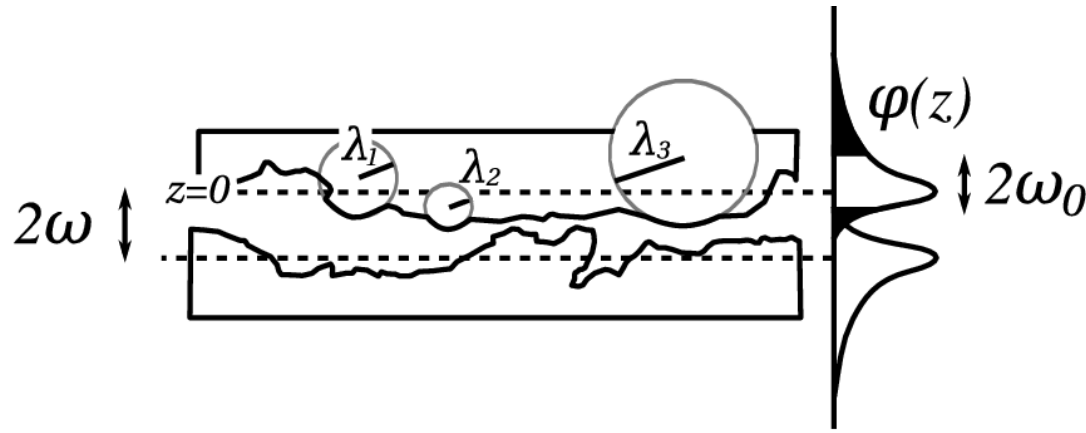


Figure 1: Illustration of ω , ω_0 and λ in the equation. $\psi(z)$ is the probability density function of the asperity heights with respect to a reference or average elevation (dotted line). Finally, ω_0 is defined as the rms of distribution $\psi(z)$ and λ as the characteristic radius in the distribution of the spherical arcs fitting individual asperities. From S. Nielsen, di Toro, and Griffith 2010

(b) The area of real contact between two rough surfaces increases proportionally to normal load. It appears that the separation ω is weakly sensitive to normal load σ_n , resulting for practical purposes in a bounded value $\omega = 2\omega_0 \rightarrow 3\omega_0$. Therefore λ can be considered as constant, and the major change upon normal load increase is than increase in the number of asperities N , but modest increase in the contact area $\pi\lambda^2$ of each individual asperity. Therefore the increase of area (and

N) is proportional to the normal load.

If friction is proportional to the real area of contact, then Greenwood (Greenwood and Williamson 1966) essentially has explained Coulomb's law of friction $\tau = \mu' \sigma_n$.

Letting α be the proportion of real contact area vs. total area, it can be shown that $\alpha = \sigma_n / \sigma_c$; the contact asperities are under a compressive stress close to the material strength σ_c , in a state of incipient plastic yield (Dieterich and Kilgore 1996; Persson 2000).

At first glance it is counter-intuitive that in point (a) above, the separation distance between the two surfaces is a highly non linear function of normal load, while the area of contact described in point (b) shows is proportional to normal load. Indeed the behavior of a distribution of asperities is quite different from that of a single, isolated Hertzian contact. One key mechanism is that, under an increasing normal load, the effective contact area increases principally by increasing the total number of contact asperities (rather than by increasing the area of existing asperities). These results are discussed at length in texts of tribology (study of friction, e.g. Greenwood and Williamson 1966; Persson 2000) but also to some extent in bibliography on fault mechanics (Brown and Scholz 1985).

In the case of fluid filling the voids between the two fault edges, we may slightly modify the above definition of α as the ratio of normal to yield stress, due to the presence of the additional pressure P in the fluid, for example, in case of melt, the pressure generated by extrusion of the viscous melt, or in case of thermal pressurization, the increase in fluid pressure due to the temperature rise. We can obtain a modified relationship by simply writing the total load across the area as the sum of two contributions:

$$\sigma_n = \alpha \sigma_c + (1 - \alpha) P \quad (2)$$

In presence of a pressurized fluid the real contact area will be smaller, in that

$$\alpha = \frac{\sigma_n - (1 - \alpha)P}{\sigma_c} \approx \frac{\sigma_n - P}{\sigma_c} \quad (3)$$

and the friction will be reduced in proportion to the pressure P such that $\tau = \mu'(\sigma_n - P)$.

(c) The contact asperities are in a state of incipient yield stress. The initial contact across a rough surface is a very tiny fraction of the total area, therefore all the normal load is concentrated to such a level that the contact yields plastically. The number of contacts gradually increases until the load is sufficiently distributed that plastic deformation slows down, but remains close to the critical yield stress (incipient yield). In such a state the contacts age, and friction continues to increase very slowly, it is shown by experimental measurements that static friction increases with the log of time (**Fig. 2**).

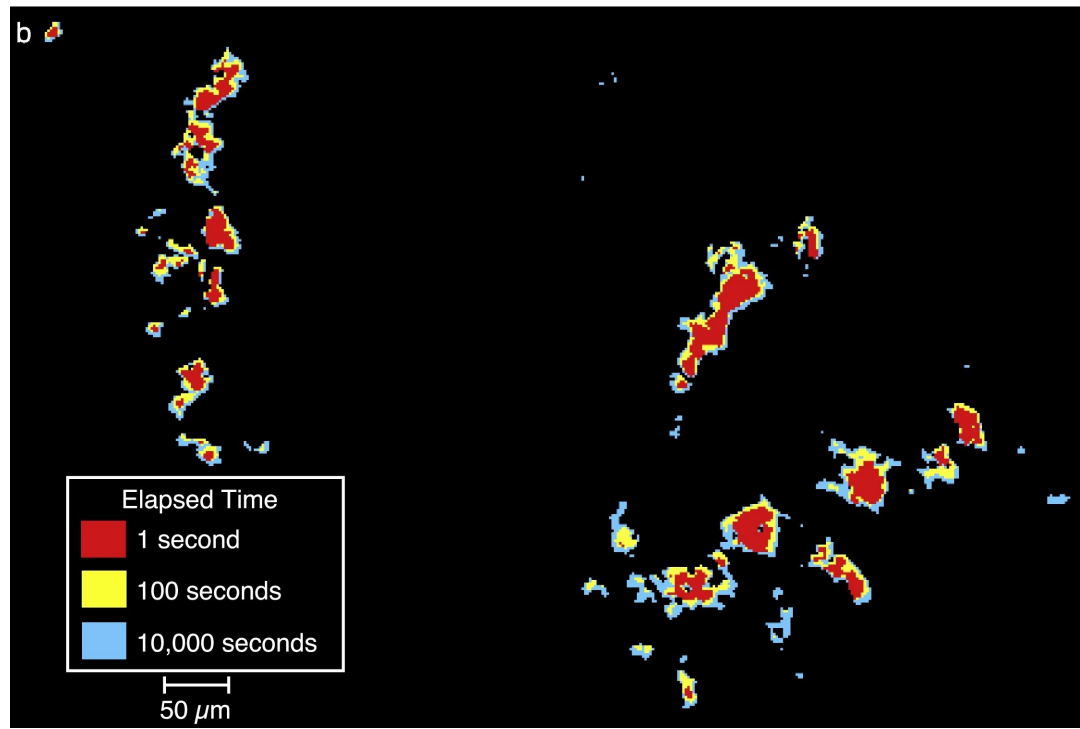


Figure 2: Example of evolution of contact asperities in time; experimental result from (Dieterich and Kilgore 1996).

(c) Sliding and abrasion. Under sliding asperity contacts will disappear and new ones will form. The average contact time will decrease with slip velocity, reducing the ageing. Contacts leave grooves on the opposite face and become

smeared in the direction of slip. This process is quite visible on either experimental friction surfaces (**Fig. 3**) and on natural faults (**Fig. 4**).

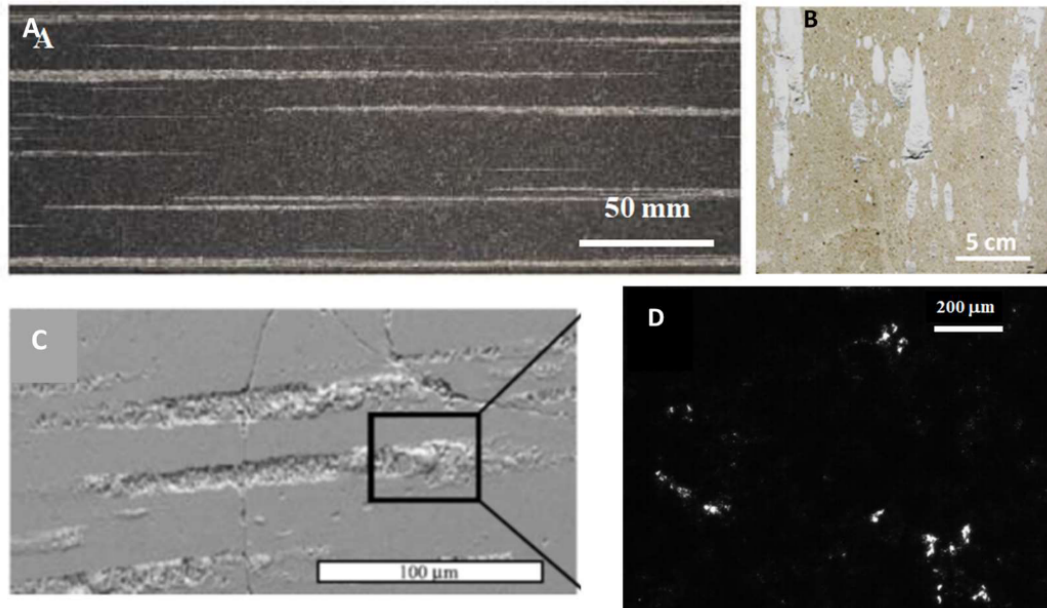


Figure 3: From (Reches, Chen, and Carpenter 2019)

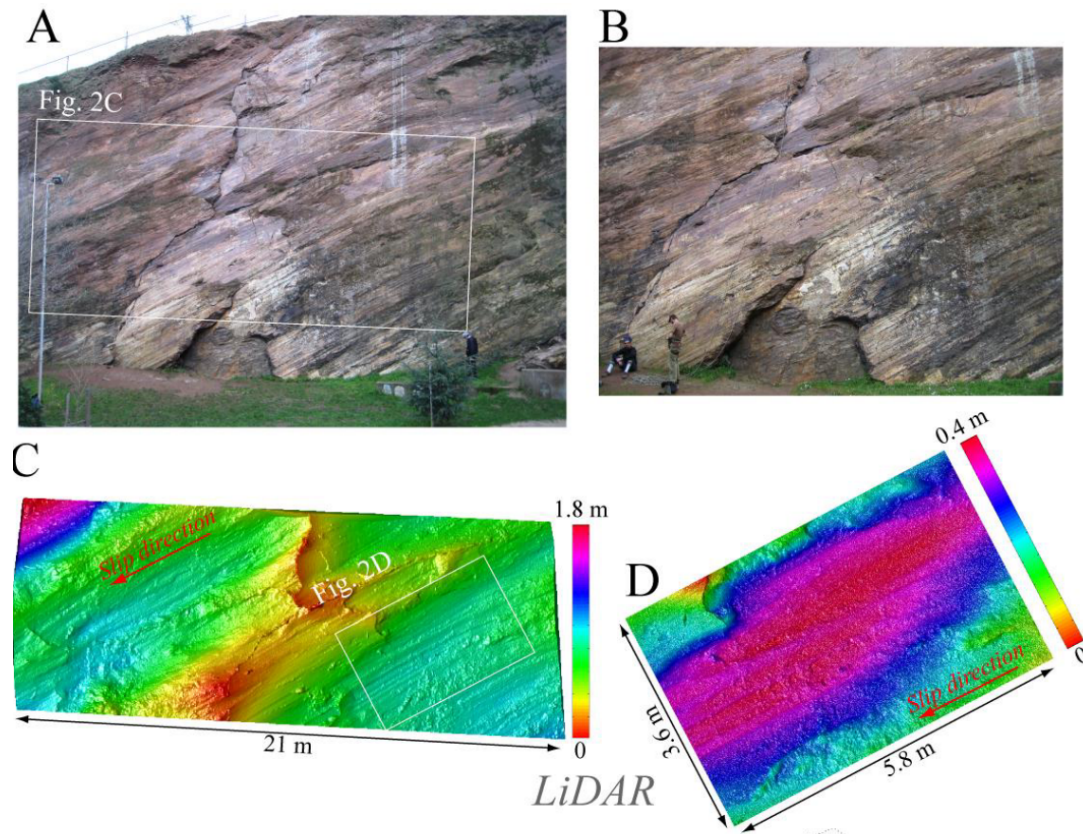


Figure 4: From (Candela, Renard, Klinger, et al. 2012)

If the sliding becomes fast, typically more than 0.1 m/s, and, in the case of seismic sliding, of the order of 1 m/s or more, the heat released by the shearing of the asperity contacts will not have much time to diffuse away from the asperity, therefore the temperature can locally rise (although the bulk temperature may still be modest). This phenomenon can induce a particular type of frictional weakening described in the *Flash weakening* section further down.

2 Effect of fault roughness on rupture triggering

One consequence of fault roughness and contact asperities, is that sections of the fault surface are devoid of any contacts. One may try to fit circular patches within non-contact areas surrounded by asperities, and find the circle with the maximum radius possible. As seen previously in eq. (??: $\pi L \frac{\Delta\tau^2}{\mu'} \geq G_c$), the rupture propagation criterion includes the half-length L of the initial fracture. Asperity-free areas being subject to no traction, they can be assimilated to initial fractures of radius L that re-distribute stress on the peripheral contacts. Increasing normal load will make new contacts appear and the size of the traction-free areas will shrink. (**Fig. 5**) As a consequence, a subtle balance between the nature of rugosity and the normal stress will regulate the potential for unstable rupture propagation on a fault (**Fig. 6**) (**Fig. 7**).

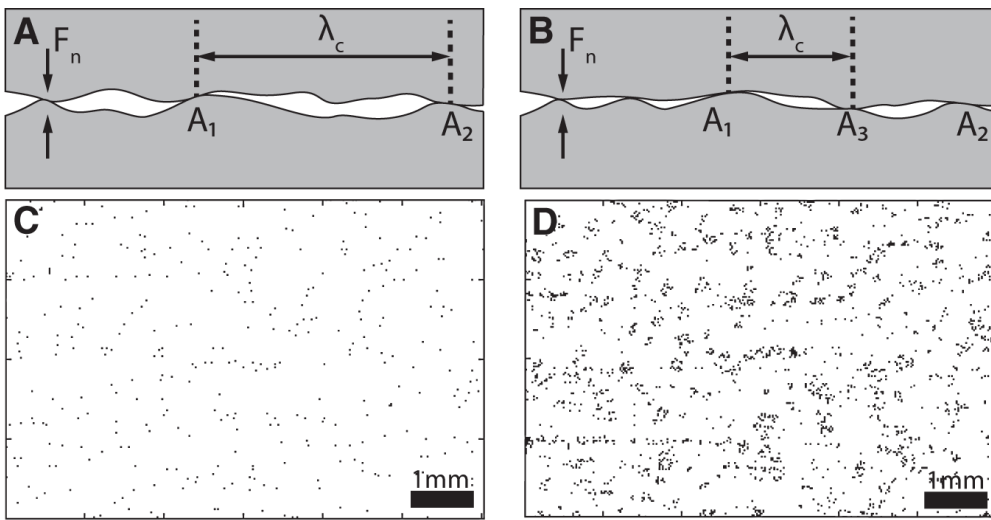


Figure 5:

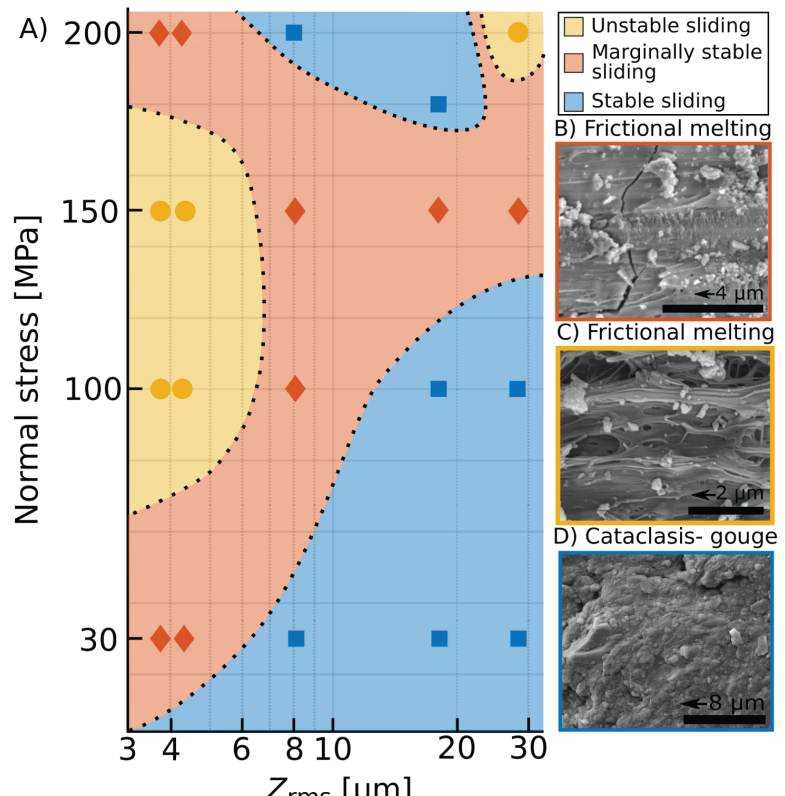


Figure 6:

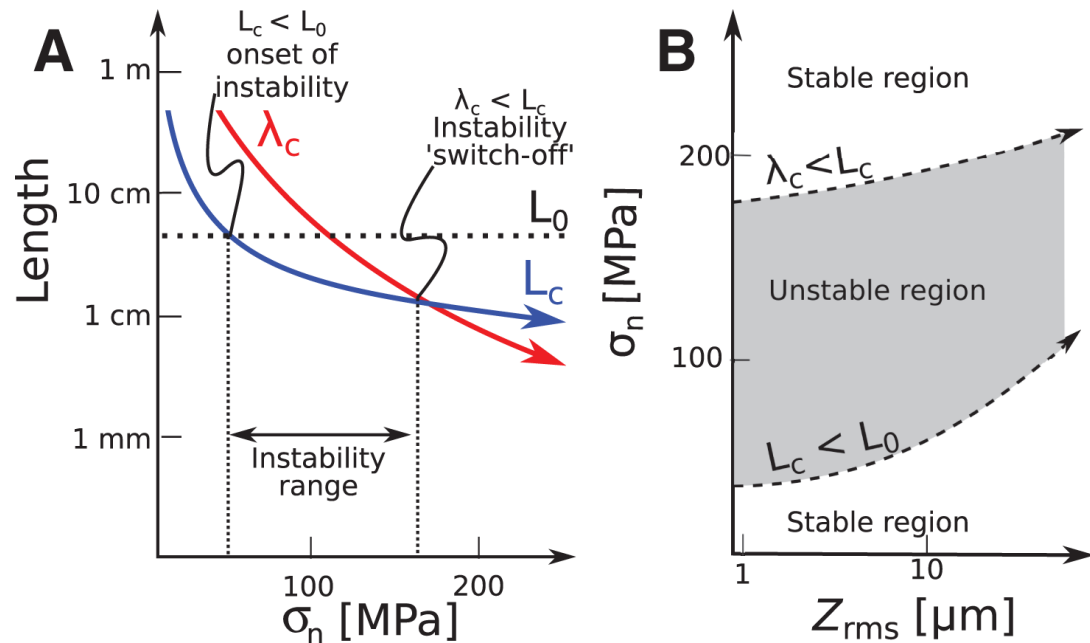


Figure 7:

3 Upscaling from micro to macro deformation –frictions on faults

- An infinitesimally thin surface? Major faults show a wide (up to hundreds of m) damage zone

- Fault structures in the field
 - Damage zone
 - Fault core
 - Principal Slip Zone (PSZ)
 - Pulverised rock
- Distributed region of plasticity vs LEFM
 - Equivalent models provided that the plasticity region is relatively small
- Models where dissipation in the volume around fracture tip is equated to frictional work on the fault
 - In what cases can this work?
 - Stress excess outside fault surface
 - Shear parallel to the fault
 - Thermally triggered, endothermal processes
 - Off-fault damage with no shear deformation.
 - Volume of contact asperities: friction is seldom a strictly surface process.
 - Dissipation from non-shearing processes, or from shearing that does not project onto the fault surface cannot be factored-in as friction, because there is no frictional work-to-slip proportionality
 - The friction-compatible work is only from shear that is compatible with double couple motion (strain tensor components on 2 orthogonal planes) and within a reasonably thin zone

- Reproducing faults in the lab
- Damage generated during the earthquake rupture

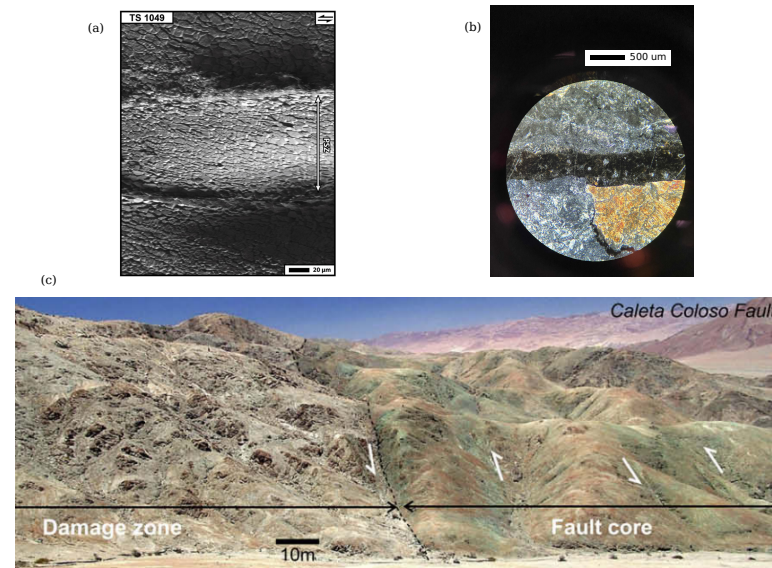


Figure 8: **The magnifying lens** Faults from the microscale to the kilometer. These are a few examples among many in the lab and in the field (from (a) (Pozzi, De Paola, Stefan Nielsen, et al. 2021) (b) Nielsen (personal collection) and (c) (T. Mitchell and Faulkner 2009)). Can we assume a zero thickness plane? If so, what is the scaling linear (just a magnifying lens) or non-linear (something fundamentally different in the dimensionless ratios at large and small scale)?

(Fig. 9) (Fig. 10) (Fig. 11)

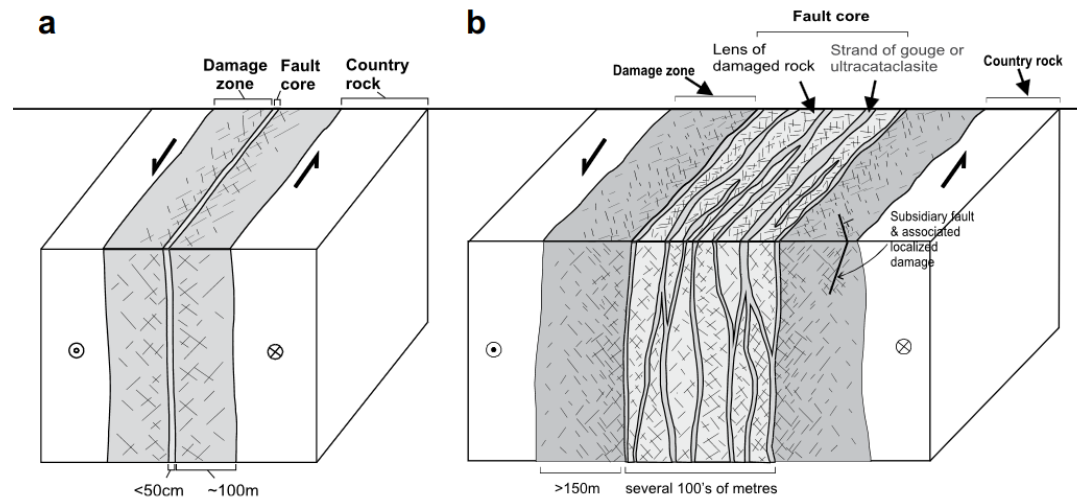


Figure 9: Form (T. Mitchell and Faulkner 2009)

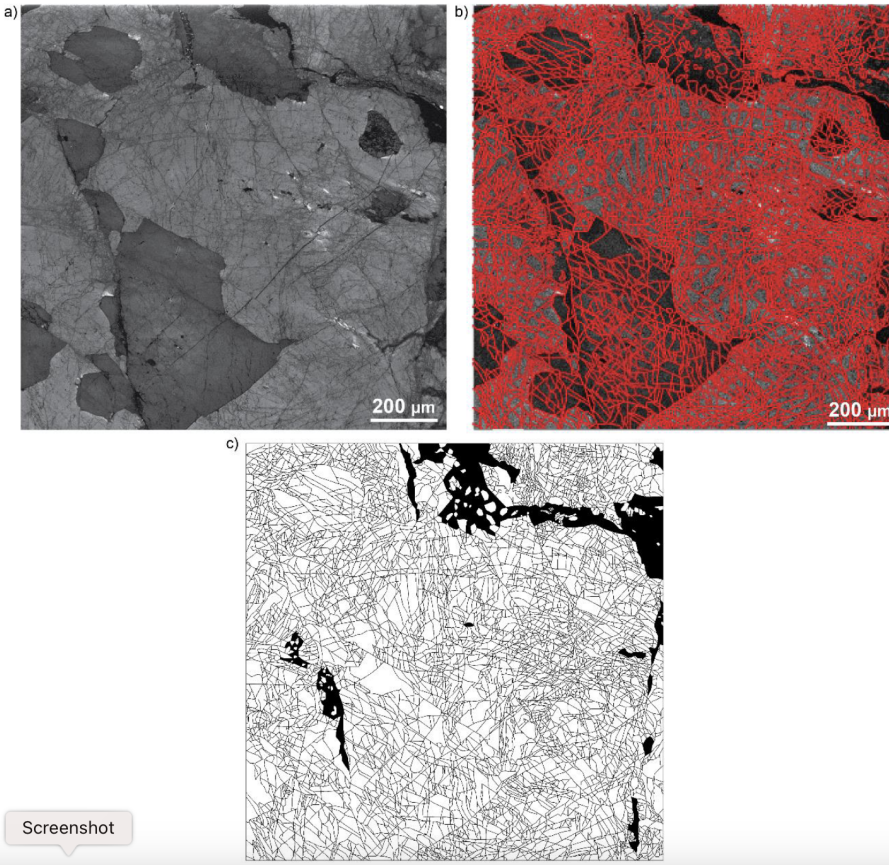


Figure 10: Form (Aldrigatti 2023)

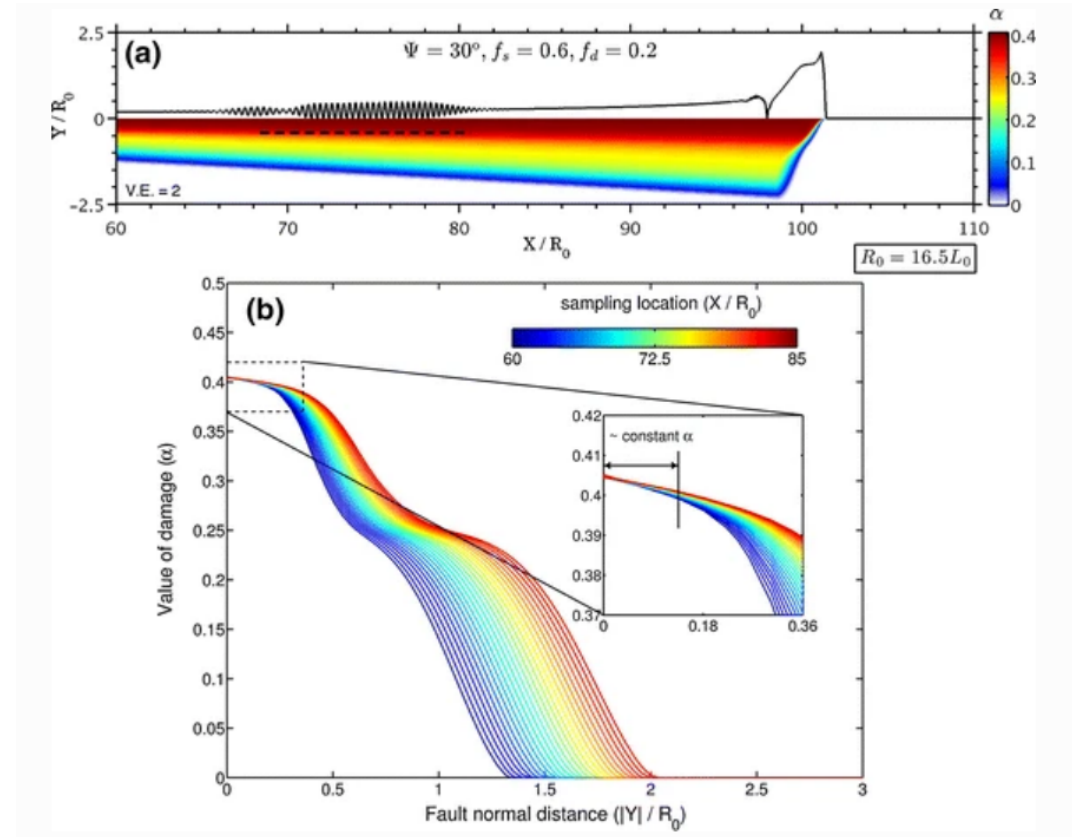


Figure 11: Form (Xu, Ben-Zion, Ampuero, et al. 2014)

4 Rupture velocity from energy considerations

Energy release rate G :

$$\begin{aligned} G &\approx \left(1 - \frac{v}{c}\right) G_0 \\ G_0 &= A_0 \frac{L \Delta\tau^2}{\mu'} \end{aligned} \tag{4}$$

(note that L , rupture length, is also rupture front position, $x_r = L$). Here G_0 is the static energy flow, and for a crack of length L . $\left(1 - \frac{v}{c}\right)$ is the Doppler approximation of Lorentz contraction. $\Delta\tau$ is the stress drop inside the crack, μ' the shear stiffness and constant A_0 is a dimensionless shape factor involving loading geometry and Poisson ratio. In addition, the initial rupture patch dimension can be defined as the critical length of a Griffith crack

$$L_c = \frac{1}{A_0} \frac{G_c \mu'}{\Delta\tau^2} \tag{5}$$

where G_c is the fracture energy. Let's replace $G_c \rightarrow \Gamma = G_c + G_{\text{off}}$ (an equivalent to G_c in the traditional LEFM sense plus any general non-local or off-fault energy dissipation G_{off}) and obtain:

$$L_c = \frac{1}{A_0} \frac{\Gamma \mu'}{\Delta\tau^2} \rightarrow \Gamma = \frac{A_0 \Delta\tau^2}{\mu'} \tag{6}$$

If we derive Γ from equation (6) and divide it by G_0 as defined in (4) we can write:

$$\frac{\Gamma}{G_0} = \frac{L_c}{L} \tag{7}$$

and note that the ratio of energy dissipation Γ to static energy flow will scale as the ratio of L_c to L .

The crack advancement criterion is that energy release rate G matches the fracture energy Γ (or energy dissipate in the advancement of crack tip):

$$G \equiv \Gamma$$

we also have (previous slide):

$$G = \left(1 - \frac{v}{c}\right) G_0 \quad \text{and} \quad \frac{\Gamma}{G_0} = \frac{L_c}{L}$$

combining these we can derive that

$$\left(1 - \frac{v}{c}\right) = \frac{L_c}{L}$$

and use $v = \partial L / \partial t$ to set the problem of rupture acceleration as the differential equation:

$$\frac{1}{c} \frac{\partial L}{\partial t} = \left(1 - \frac{L_c}{L}\right)$$

This extremely simple solution immediately illustrates (a) self-similarity in the ratio L_c/L , and that (b) rupture velocity at fixed L is a decreasing function of L_c , in other words, larger break-out patches will accelerate more gradually.

Furthermore, we can solve (4) for $L(t)$ to yield

$$L(t) = L_c \left(1 + W_0 \left[\exp \left(\frac{C_{lim}}{L_c} (t - t_0) \right) \right] \right)$$

where W_0 is the principal branch of the Lambert W function, and t_0 an arbitrary integration constant or reference time. The significance of t_0 is that $L = L_c$ is perfectly matched only at time $-\infty$, and that an hypothetical breakout patch infinitely close to instability would take an infinite time to accelerate in the absence of finite perturbations.

Note that the asymptotic behavior of (4) at large time can be obtained as

$$\lim_{t \rightarrow \infty} L(t) = L_c + C_{lim} (t - t_o) \quad (8)$$

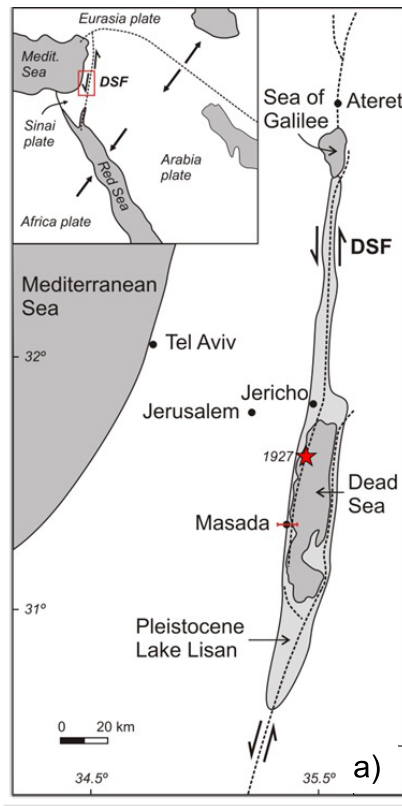
i.e., a constant rupture velocity at the limit speed C_{lim} , under the assumption that no supershear rupture transition has yet occurred.

5 An example of off-fault damage

- Rupture propagation in poorly consolidated sediments: lab and theoretical energy perspective
- Rupture at the trench: the analogous case of Lisan faulting

Motivation : tsunami earthquakes

- Shallow ruptures in soft, clay-rich sediments have slow rupture velocity and low radiation efficiency.
- Ruptures are known to nucleate and propagate within the accretionary prism.
- Despite low radiation, they pose risk of tsunamis and are referred to as "tsunami earthquakes" (Kanamori).
- Tsunami earthquakes trigger a significantly greater tsunami than expected for the magnitude predicted from shorter-period seismic waves (Nicaragua 1992, Java 1994, Guerrero 2002, and many others...)
- They are particularly dangerous as a large tsunami may arrive at a coastline with little or no warning.



- N-S strike, sub-parallel to the main graben-bounding structures
- Faults cut through 30 metres thick Pleistocene Lisan Formation sediments in (dried) Lake Lisan
- The Lisan sediments were subaqueous at the time of deformation and are very poorly lithified
- They do behave as a cohesive and elastic rock, although the strength is very low

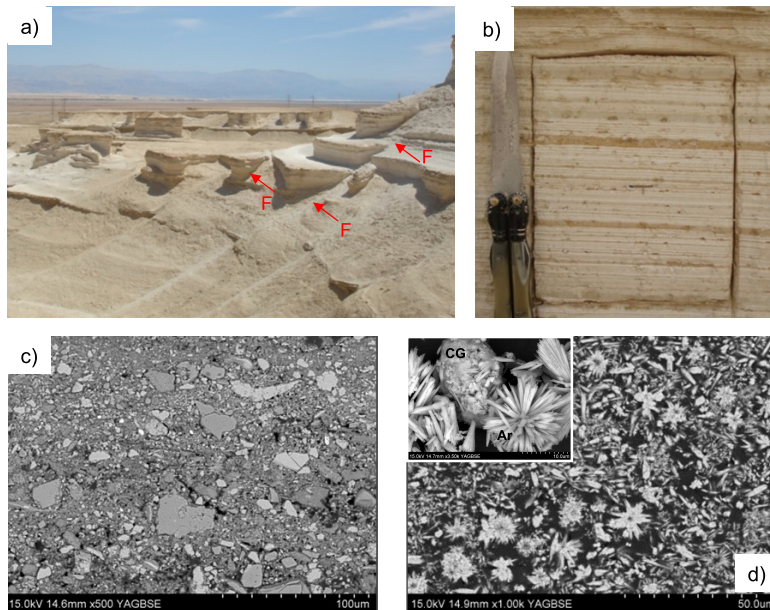
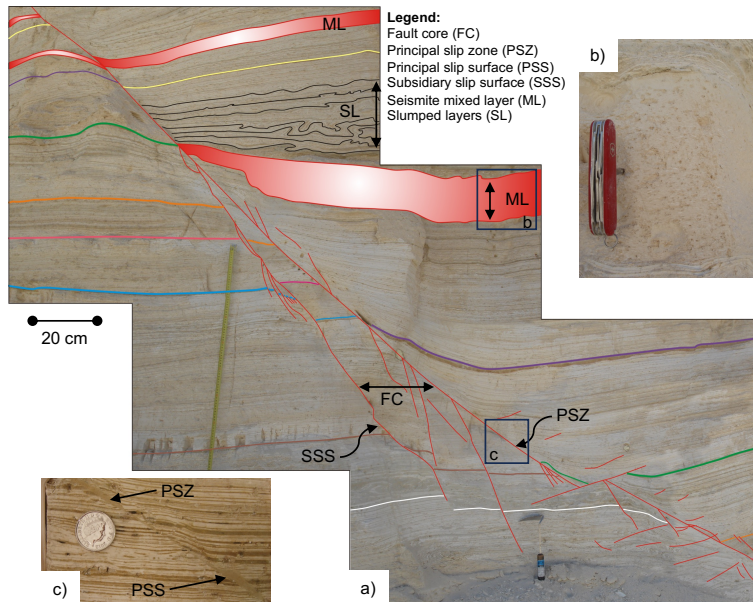


Figure 12: From Bullock et al., in press *Nature Comm.*



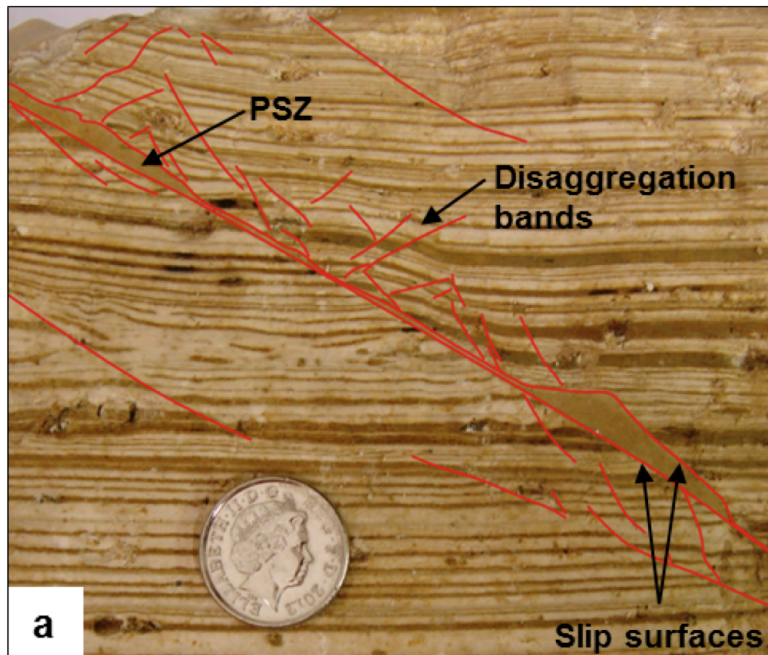
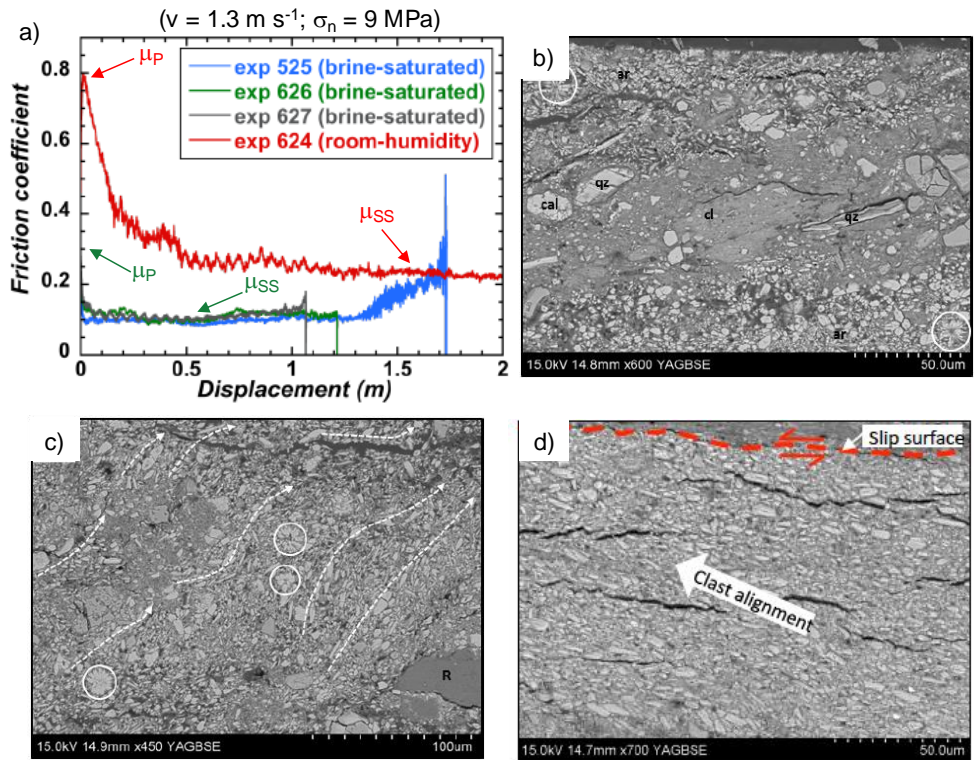


Figure 14: From Bullock et al., in press *Nature Comm.*



Energy Dissipation in Fault Arrays

For each individual shear structure, the incremental energy dissipated by slip is

$$dE_{D,i} = \tau_i(d) dd,$$

and thus the total dissipated energy on all N shear structures of the array is

$$E_D = \sum_{i=1}^N \int_0^{d_i} \tau_i(d) dd,$$

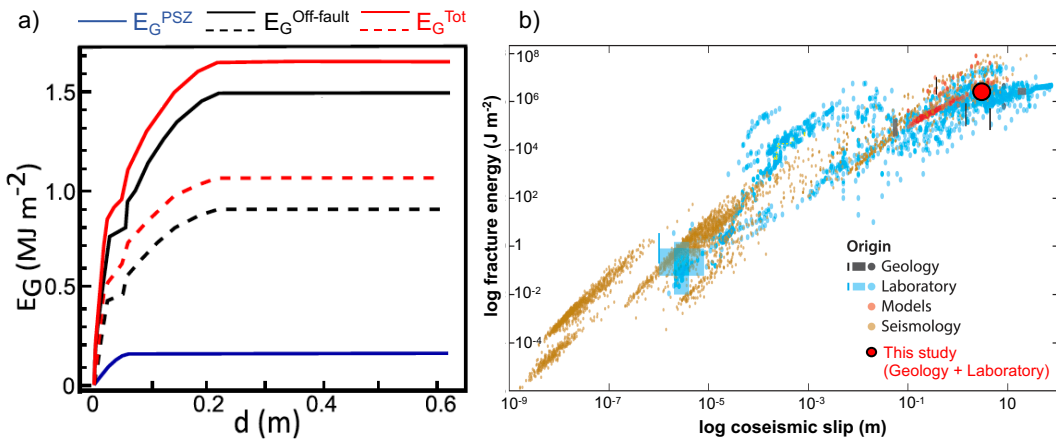
where $\tau_i(d)$ is the shear stress acting on the i -th structure as a function of slip d , and d_i is the final slip.

The total dissipated energy E_D can be partitioned into the sum of residual frictional work E_F and fracture energy E_G :

$$E_D = E_F + E_G,$$

where τ_r si the minimum residual frictional level (below base of triangle), such that $E_F = \sum_{i=1}^N \tau_r d_i$, and d_r is the slip on the i -th structure. Therefore, the off-fault fracture energy can be written as

$$E_G^{\text{Off-fault}} = \sum_{i=1}^N \int_0^{d_i} [\tau_i(d) - \tau_{r,i}] dd,$$



From the fault observations and the lab measurements, the resulting values are

$$E_G^{\text{PSZ}} = 0.16 \text{ MJ m}^{-2},$$

$$E_G^{\text{Off-fault}} = 0.9 \text{ to } 1.5 \text{ MJ m}^{-2}$$

$$\Gamma = (E_G^{\text{PSZ}} + E_G^{\text{Off-fault}}) = 1.06 \text{--} 1.66 \text{ MJ m}^{-2}$$

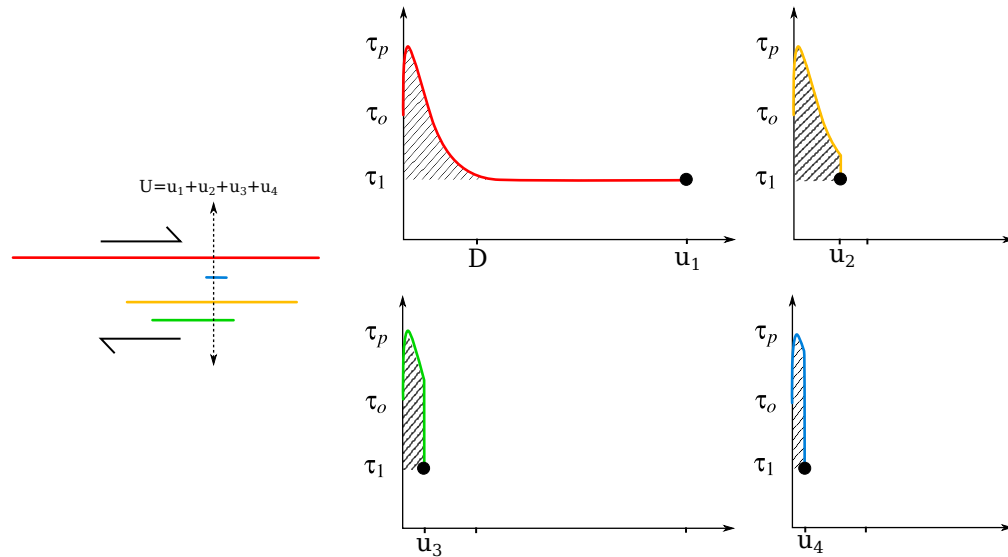


Figure 17: From Bullock et al., in press *Nature Comm.*

6 Rupture scenarii from lab and field measurements...

Can we use the above results on dissipation to estimate rupture velocity?

Reminder.... From stress intensity to energy flow

From Fossum and Freund (1973), the stress intensity factor at time t can be written as

$$K(t) = \int_0^{L(t)} \frac{\Delta\tau(x)}{\sqrt{L(t)-x}} dx, \quad (9)$$

where $L(t)$ is the current rupture tip position at time t , and $\Delta\tau(x)$ is the local stress drop at position x , that is, the location along the fault trace.

Assuming that x is the up-dip position along the fault, and using piecewise constant prestress (τ_1 for the fault root from 0 to L_1 , and τ_2 for the shallow part from L_1 to L), we can write

$$K = \int_0^{L_1} \frac{\tau_1}{\sqrt{L-x}} dx + \int_{L_1}^L \frac{\tau_2}{\sqrt{L-x}} dx, \quad (10)$$

which gives

$$K = 2 [\tau_1 \sqrt{L-L_1} + (\tau_2 - \tau_1) \sqrt{L-L_1}], \quad (11)$$

for $L > L_1$.

From the stress intensity factor, we can compute (Broberg, 1990) the energy release rate G for a crack propagating at vanishingly small velocity in plane-strain conditions as

$$G = \frac{(1-\nu^2)}{E} K^2, \quad (12)$$

where E is Young's modulus and ν is Poisson's ratio.

Reminder.... From energy balance to rupture velocity

$$G(v) = G_0 \frac{\sqrt{1-\gamma^2}}{1+\gamma}, \quad G_0 = A_0 \frac{K_0^2}{2\mu'}$$

Finally, the approximation is obtained by

$$\lim_{\gamma \rightarrow 0} \frac{\sqrt{1-\gamma^2}}{1+\gamma} = 1-\gamma, \quad G(v) \approx G_0(1-\gamma)$$

$$\begin{aligned} G(v) &\approx \left(1 - \frac{v}{c}\right) A_0 \frac{K_0^2}{2\mu'} \\ &\approx \frac{(1 - \text{Poisson})}{2\mu'} \left(1 - \frac{v[L]}{c}\right) \left[2\tau_1 \sqrt{L-L_1} + 2(\tau_2 - \tau_1) \sqrt{L-L_1}\right]^2 = \Gamma[L] \end{aligned}$$

Solve for rupture velocity $v[L]$ as a function of $\Gamma[L]$ (the dissipation due to friction + off fault damage)...

We now have:

- An approximate solution for rupture velocity in a medium of inhomogeneous stress drop and fracture energy
- A field estimate of slip partition on an array of n faults, including the principal slip zone
- A laboratory estimate of peak friction, residual friction and weakening curve for the fault host rock (allowing to estimate the dissipated energy in each fault of the array)
- A global dissipation obtained by summing the n faults of the array

We can compute rupture propagation in the poorly lithified layer, that we may arguably use as an analogue for the accretionary prism on trench faults (?).... What do we get?

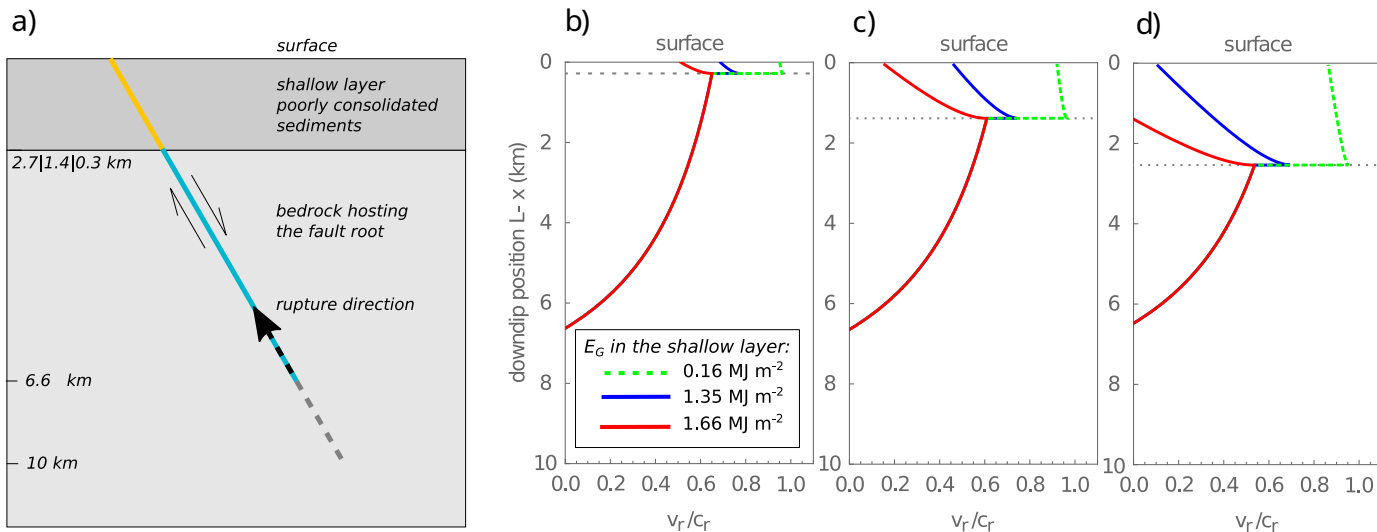


Figure 18: Rupture scenarii with different thicknesses of poorly lithified sediments (top layer). The assumption is that the top layer has *no initial shear stress*, $\tau_0 = 0$ (not capable of cumulating tectonic load). Nonetheless, rupture can push through this layer due to the energy flow coming from the bottom layer. The peak and residual stress values were obtained experimentally as $\tau_p = 6.07$ MPa, $\tau_r = 0.9$ MPa, as was the fracture energy in the top layer (≈ 1.35 MJ m⁻¹). The prestress and the fracture energy in the bottom layer were assumed using indicative crustal values of 3 MPa 1 MJ, respectively.

Sliding friction at slow slip rates

A very large body of literature exist that has explored the rate and state laws both theoretically and experimentally –Alan Rubin to gave a much more complete overview, but to recall the general formulation, we can write:

$$\begin{aligned} \mu &= \mu_0 + a \log \frac{V}{V_0} + b \log \frac{\theta V_o}{D_c} \quad (a) \\ \frac{d\theta}{dt} &= 1 - \frac{V \theta}{D_c} \quad (b) \\ \mu_{ss} &= \mu_0 + (a - b) \log \frac{V}{V_0} \quad (c) \text{ (steady-state limit)} \end{aligned} \quad (13)$$

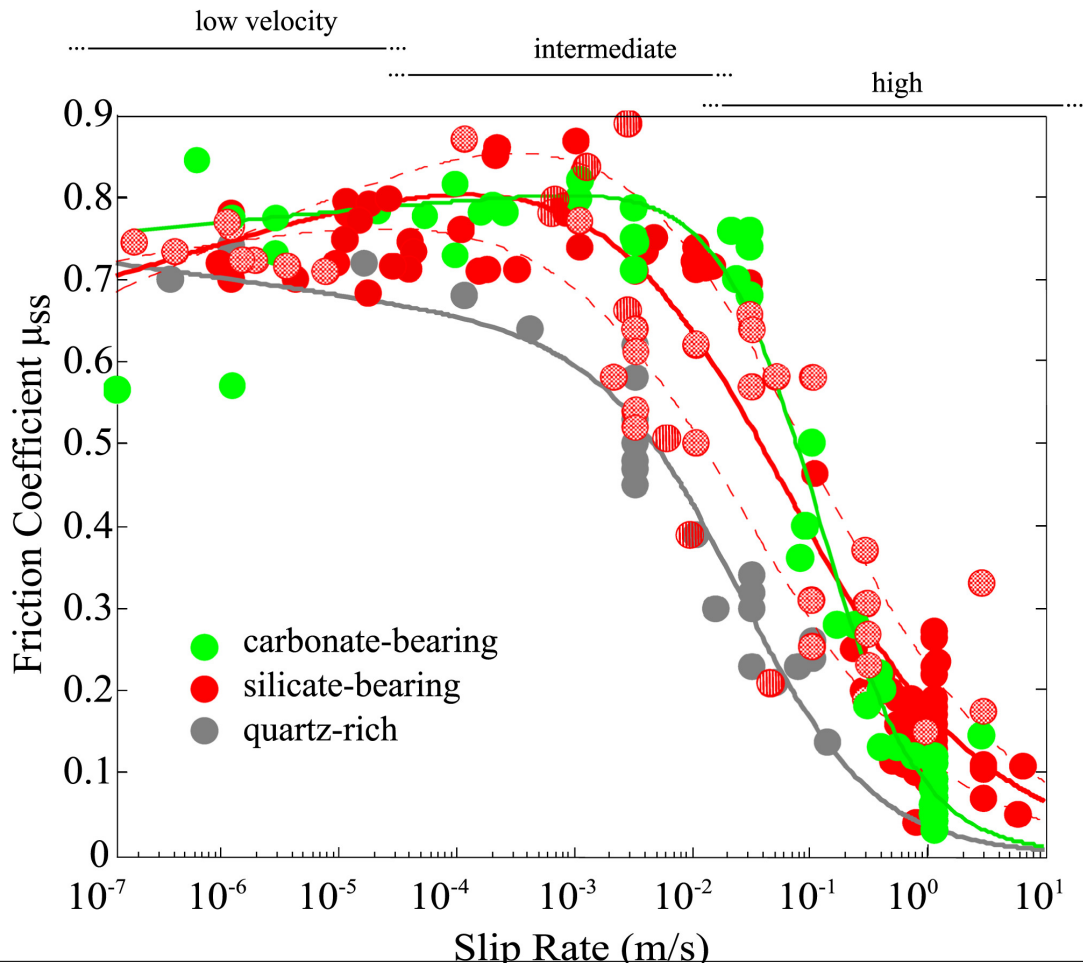
(Alternatives with other evolution laws for θ exist). The rate-and-state laws reproduce well experiments in the range 1-500 $\mu\text{m/s}$, and allow to simulate, among other things, the nucleation phase of earthquakes and a rich spectrum of fault behaviour from stable creep to unstable slip episodes and earthquakes.

The steady state condition allows defining a critical stiffness:

$$\begin{aligned} K_c &= \frac{\sigma_n V}{D_c} \left(\frac{d\mu_{ss}}{dV} + F(V, \theta_f) \right) \\ &= \frac{\sigma_n (b - a)}{D_c} \quad (\text{no inertia}) \end{aligned} \quad (14)$$

where σ_n is the effective stress normal to the fault and $F(V, \theta_f)$ is a generic term for inertia. When a slider bloc or, by analogy, a fault has $K < K_c$ then it can accelerate and become unstable, which might generate a slow or a fast earthquake (where the fault stiffness can be defined as $K = \mu'/L$).

At high slip velocity (typically $V > 0.1$ m/s) dramatic frictional weakening is observed 19 that cannot be simulated by the modest logarithmic velocity dependence of (13) (**Fig. 19**).



Rupture scenarii from lab and field measurements...

Because the velocity dependence at high slip rates in a variety of fault rock materials appears to a good approximation to behave as negative power-law of velocity, an empirical fit can be obtained by combining(13) with a velocity denominator such that:

$$\mu = \frac{\mu_0 + a \log \frac{V}{V_0} + b \log \frac{\theta V_o}{D_c}}{1 + (V/V_c)^p} \quad (15)$$

An alternative, and more general definition of critical stiffness can then be derived, that allows for instability in a wider range of parameters (Spagnuolo, S. Nielsen, Violay, et al. 2016).

Exercise:

Assuming that a fault at a plate boundary is under stable sliding at 10 mm/y (plate motion). During an earthquake there is a stress drop from 60 to 20 MPa when the fault slip accelerates. Estimate the slip velocity that would generate an equivalent friction drop during the earthquake, assuming that a rate and state friction as (13-c) is acting. Assume that the fault depth is at 3 km depth, that the rock density is $\rho = 2800 \text{ kg m}^{-3}$. Use representative values of $a - b = -0.004$ for a rate-weakening rock. Repeat the estimate using 15 with $V_c = 0.05 \text{ m/s}$ and $p=1$. In which case the fault slip acceleration is more realistic?

There is a fundamental change in the frictional slip at rates above a few cm/s. The main reason is the temperature rise that takes place when high power from frictional slip produces heat at a faster rate than could be efficiently be evacuated by diffusion. In the coming section we will analyse a few processes where heating is responsible for enhanced weakening.

Sliding frictions at fast slip rates:

As roundly summed up by (Madariaga 2007), one can consider that earthquake faults are *slippery when hot*. Effectively the heat is generated by the sliding itself, and there are several ways that temperature rise can weaken the dynamic sliding friction.

The heat rate (or power) of frictional sliding under a shear stress τ and velocity V

$$q(t) = \frac{1}{2}(\tau(t)V(t) - q_s(T(t))), \quad (16)$$

where τ is shear stress, V is sliding velocity, and q_s represents thermally triggered energy sinks (e.g., latent heat, etc); q is introduced as a heat source on the fault surface, represented in the 1D thermal diffusion equation (z is the fault-perpendicular direction):

$$\partial_t T = \kappa \partial_z^2 T + \frac{\delta(z)}{\rho c} q; \quad (17)$$

finally, the temperature of the fault surface resulting from the solution of (17) will have a feedback effect on the shear stress τ , assuming that it has a thermal dependence:

$$\tau(t) = f(V, T, \dots) \quad (18)$$

Therefore the 3 above equations are coupled in the frictional weakening problem.

Exercises:

- 1) The penetration depth of a diffusive process is of the order of $z = \sqrt{2\kappa t}$. Do a back-of-the-envelope calculation of average temperature within z for the conditions of question (1),

after 0.1 s, 1 s, 2 s, 10 s. Assume a shear stress of 10 MPa, a sliding velocity of $V=1$ m/s and a diffusivity of $10^{-6}\text{m}^2\text{s}^{-1}$.

- 2) Compute the temperature rise vs. time on the fault surface ($z=0$) for the same conditions as above.
- 3) Compute the temperature profile perpendicular to the fault after the same time intervals as question (1).

Useful equations:

The well-known solution of the diffusion equation Carslaw and Jaeger 1990 for a heat flow Φ imposed at the border of a half-space is obtained by integrating

$$T(z,t) = \frac{1}{\rho c \sqrt{\kappa \pi}} \int_0^t \frac{\Phi(t')}{\sqrt{t'}} e^{-z^2/(4\kappa t')} dt'$$

which, for a fixed flow $\Phi = \tau V$, yields the temperature profile:

$$T(z,t) = \left(\frac{2e^{-\frac{z^2}{4\kappa t}} \sqrt{t}}{c\rho \sqrt{\pi \kappa}} - \frac{z \operatorname{erfc}\left(\frac{z}{2\sqrt{\kappa t}}\right)}{\kappa \rho c} \right) \frac{\tau V}{2}$$

A foreword on experimental techniques

It is challenging to conduct experiments at high velocity, and the technical breakthroughs were achieved between the eighties and the early 2000s.

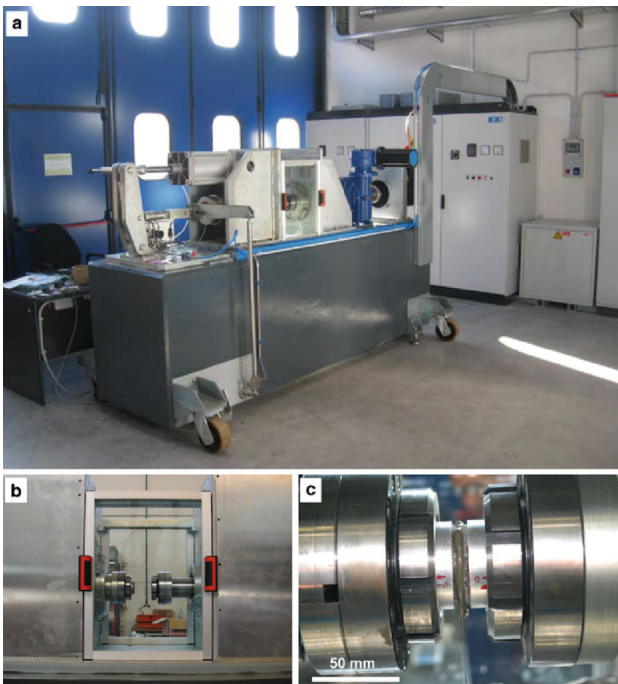


Figure 20:



Figure 21:



Figure 22: From Pozzi et al. 2021.

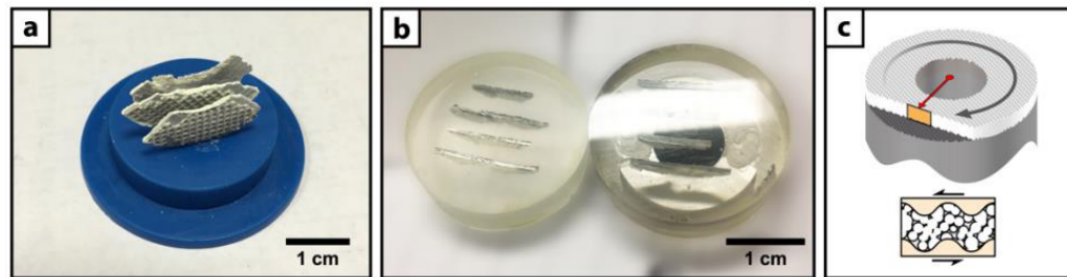


Figure 23: From Pozzi et al. 2021.

Play **VIDEOS** showing experiments at HV

Flash weakening

Flash weakening and heating of contact asperities has been proposed as a model for high velocity friction evolution (Archard 1959; J. R. Rice 2006). There are strong experimental indications (Goldsby and Tullis 2011; Violay, Di Toro, S. Nielsen, et al. 2015) that this model is relevant for high velocity experiments, in both silicate- and carbonate- built rocks, at least in the first millimeters of slip or until melting or decomposition of the rock minerals creates an almost continuous, amorphous interstitial layer. One motivation to explore flash heating is that weakening precedes the substantial rise of the background temperature of the sliding interface. Initial thermal weakening may be achieved only if local temperatures $T + \Delta T$ at asperity contacts are much higher than the background temperature T (**Fig. 24**).

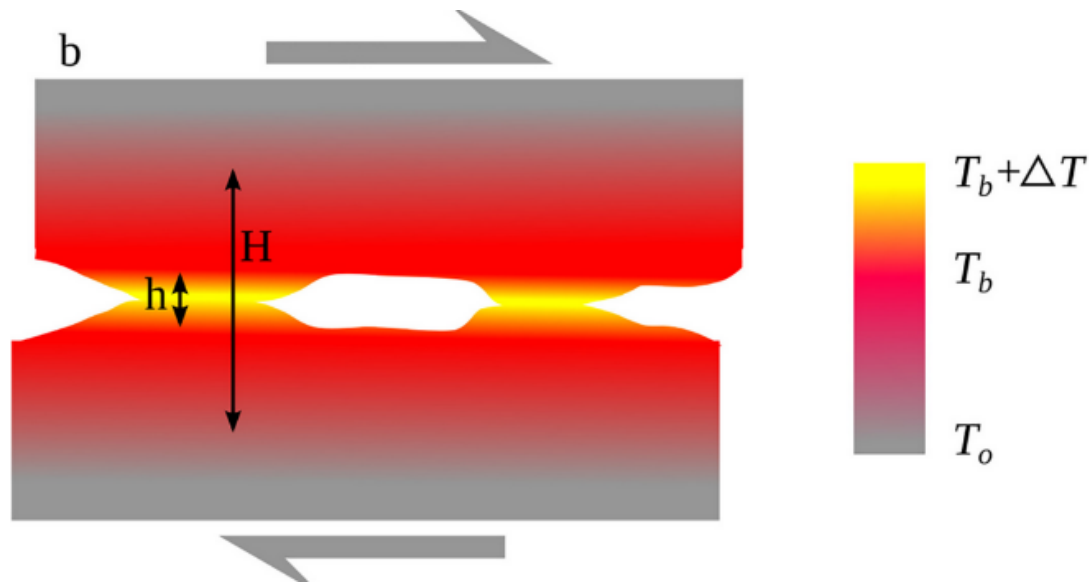


Figure 24: Local temperature rise at contact asperities can weaken friction very effectively and much earlier than the rise of bulk temperature becomes consistent. From (S. Nielsen, Spagnuolo, Violay, and G. Di Toro 2021)

The FW model considers that the lifetime of asperity of linear dimension D is indicatively $t_c = D/V$. For an asperity sheared under incipient yield stress τ_c , the heating results from frictional power $\tau_c V$. Assuming that heat diffusion is mostly perpendicular to the fault, during the asperity lifetime, with $q \approx \tau_c V = \text{const.}$ the local temperature rise is $\Delta T = \gamma \tau_c V \sqrt{t_c} = \gamma \tau_c \sqrt{V D}$, and the time during contact at which the asperity weakens is $t_w = (T_w - T)^2 / (\gamma \tau_c V)^2$. Upon defining a threshold temperature $T_w = T + \Delta T$, a minimum slip rate V_w can be computed at which shear resistance is lost

within the duration of an asperity contact lifetime:

$$V_w = \frac{1}{\gamma^2 \tau_c^2 D} \text{Max}[T_w - T, 0]^2 \quad (19)$$

The average strength of an asperity contact during its lifetime will be $\tau_a = (\tau_r(t_c - t_w) + \tau_c t_w)/t_c$, where τ_r is the residual shear stress supported by the weakened asperity. Assuming an asperity population with dominant dimension D , using $\tau_p = \alpha \tau_c$, $\tau_w = \alpha \tau_a$, $\tau = \alpha \tau_a$ and noting that $t_w/t_c = \tau_c (T_w - T)^2 / (\gamma^2 \tau_c^2 V D) = \tau_c V_w / V$ it is found (J. R. Rice 2006) that the effective sliding shear stress is:

$$\tau \approx (\tau_p - \tau_w) \left(\frac{V_w}{V} \right) + \tau_w \quad (20)$$

for $V > V_w$. We find, however, that the onset of weakening (first centimeters of slip) in the experiments is smooth and better reproduced by the regularised form:

$$\tau \approx (\tau_p - \tau_w) \left(\frac{V_w}{V + V_w} \right) + \tau_w \quad (21)$$

which can be used for all V . This may qualitatively reflect the behaviour of a distribution of asperities whose weakening is gradually triggered at different velocities depending on their size, rather than an abrupt onset of weakening of all asperities at the same threshold velocity V_w .

One of the peculiarities of the model described by equations (20) is the absence of explicit dependence on normal stress. However, the evolution of background temperature T can be factored into (19), rather than using a constant V_w . Thus the effect of τV as a heat source implicitly includes normal stress, which will reflect on the temperature rise and therefore on the velocity weakening through V_w .

Indeed during the initial part of the slip $\tau = \tau_p = \mu_s \sigma_n$ where μ_s is the initial friction coefficient (of the order of 0.6 before onset of weakening). Thus, although the initial (peak) stress will be higher under higher normal stress, temperature rise and weakening will be accelerated by a similar proportion. As a consequence, the weakening slip distance and the fracture energy may not be significantly altered by a change in normal stress. This behaviour was indeed observed in a synthesis of different high velocity friction laboratory experiments (S. Nielsen, Spagnuolo, Violay, S. Smith, et al. 2016; S. Nielsen, Spagnuolo, S. A. F. Smith, et al. 2016).

Physical models that reproduce weakening due to thermal effects can take into account different processes, such as (1) the flash weakening model for the instantaneous velocity dependence, and (2) the thermal diffusion to simulate the bulk temperature evolution, and (3) the presence of heat sinks due to phase transitions that are triggered by the temperature rise. All three effects are taken into account in (S. Nielsen, Spagnuolo, Violay, and G. Di Toro 2021) where experimental weakening curves are reproduced numerically as shown in (Fig. 25).

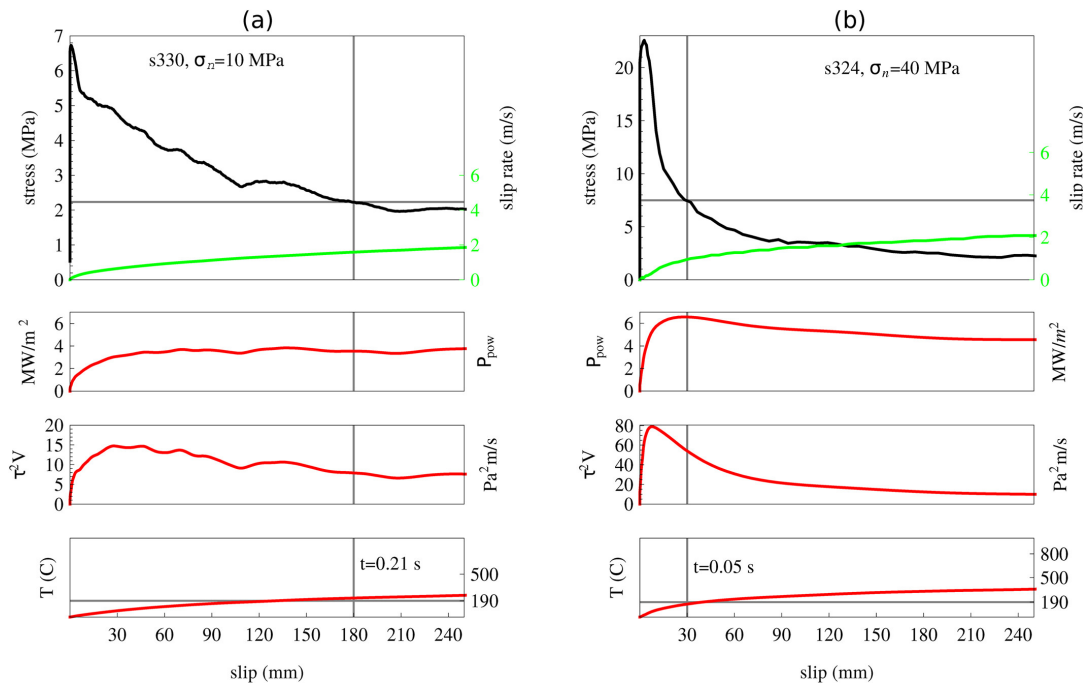


Figure 25:

Looking for a supporting argument for the role of bulk temperature in frictional weakening, and to verify the numerical model, (S. Nielsen, Spagnuolo, Violay, and G. Di Toro 2021) did two experimental test that were identical, except in one case the sample was cooled by immersion in liquid Nitrogen. The initial temperature of the sample, in the region around

the frictional sliding surface, was estimated at $-140 < T_i < -50^{\circ}\text{C}$. The mechanical curves obtained from the tests (**Fig. 26**) show a delayed weakening in the case of the cooled sample (**Fig. 26**) –the weakening is reproduced reasonably well by the model by using an initial temperature $T_i = -70^{\circ}\text{C}$, which is compatible with the estimate.

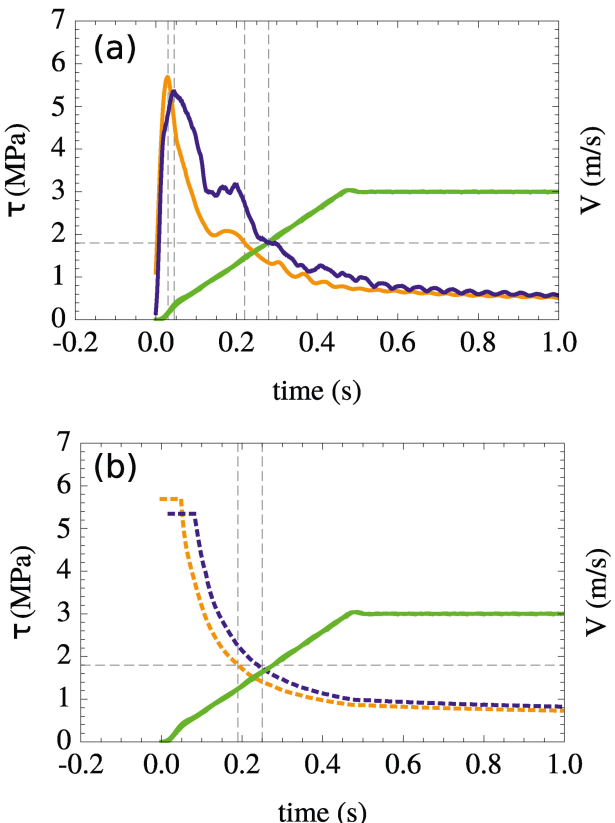


Figure 26: From (S. Nielsen, Spagnuolo, Violay, and G. Di Toro 2021)

Superplasticity

7 Large anelastic strain and plasticity

Anelastic deformation can be modelled, for example, by Arrhenius-type flow laws that generally depend on grain-size D and on temperature T (Pozzi, De Paola, Stefan Nielsen, et al. 2021). The shear strain-rate $\dot{\gamma}$ and the shear stress τ on a fixed plane and direction can be equated by:

$$\tau^n = C \dot{\gamma} e^{\frac{H}{RT}} D^b \quad (22)$$

where H is creep activation energy and C a dimensional normalisation factor. In the case of grain boundary sliding the exponents are $n = 1$ and $2 < b < 3$, with slightly increasing values if dislocation creep component is present. These laws generally fall under the behaviour of non-Newtonian viscosity, however, if $n = 1$ we can assimilate the flow to viscous shear such that $\tau = \eta \dot{\gamma}$ where the equivalent instantaneous viscosity is $\eta = C e^{\frac{H}{RT}} D^b$.

Anticipating on further section of this paper, we note that the shear stress τ is exponentially proportional to the inverse of temperature T . Therefore larger temperatures may allow high strain rates to be accommodated under relatively low shear stress. Because the dissipation induced by flow will increase the temperature, one can foresee that flow will promote the weakening of the solid (or fluid) where deformation occurs. Weakening in frictional slip is important in the context of earthquakes because it can promote unstable sliding and favour earthquake rupture propagation.

Exercise:

Estimate the temperature increase necessary to drop the shear stress to 50% of its initial value, assuming $\frac{H}{R} \approx 10^4 \text{ }^\circ\text{K}$, $T_{ini} = 2200 \text{ }^\circ\text{K}$, $n = 1$ and a fixed shear rate and D .

It is known that crystal plasticity, under favourable circumstances, can be described by flows laws such as (22) extrapolates to extreme conditions of shear rate. Usually experimentally measured at conditions of $\dot{\gamma} \ll 1$, but they have been verified at $\dot{\gamma} \approx 1$, a conditions known as superplasticity.

Having observed structures typically formed under a crystalline plastic flow known as grain boundary sliding (GBS), on samples of calcite sheared at seismic conditions (**Fig. 27**), Pozzi, De Paola, Stefan Nielsen, et al. 2021 set out to verify experimentally whether flow laws could explain the extreme weakening at high speed and whether different types of rock could be behave differently.

If a flow law can indeed be extrapolated, it is likely to be governed by different, and yet unkown parameters than those esimated for low strain rates. However, a general signature of the thermal dependance is expected, and can be highlighted by taking the log of 22 such that

$$\log \tau = \left(\frac{H}{n R} \right) \frac{1}{T} + \frac{1}{n} \log \frac{\dot{\gamma} D^m}{C} \quad (23)$$

and noting that regardless of the values of H, n, m, C , a loglinear form should be observed such that

$$\log \tau = A \frac{1}{T} + B. \quad (24)$$

(Fig. 27), (Fig. 28), (Fig. 29)

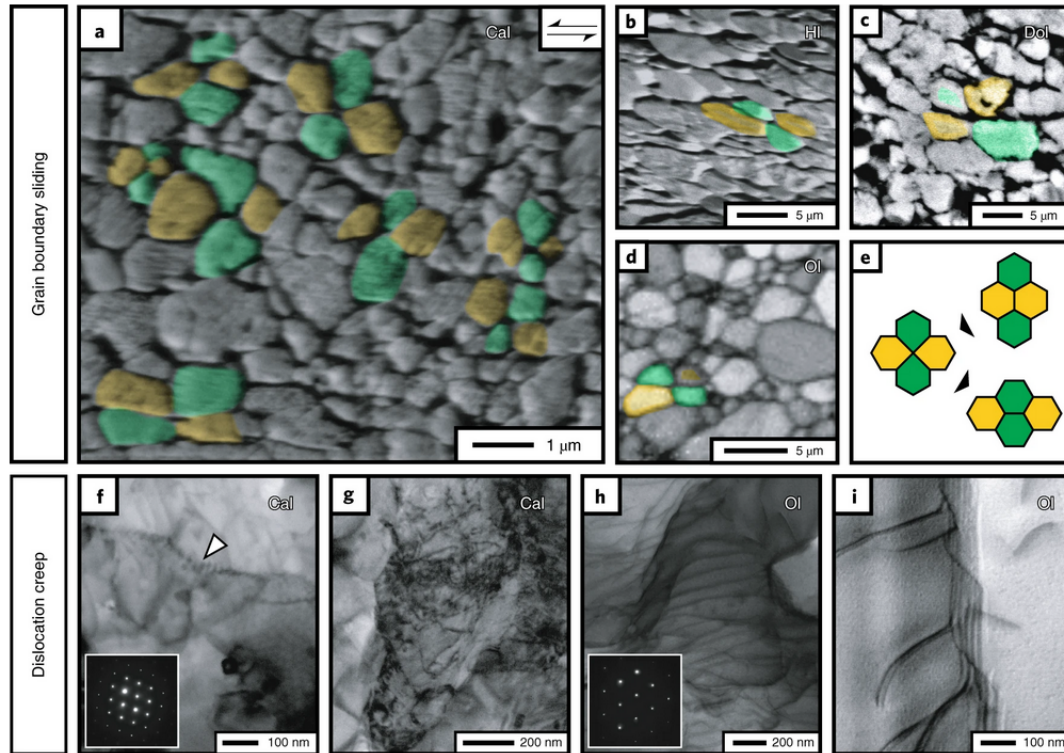


Figure 27: From (Pozzi, De Paola, Stefan Nielsen, et al. 2021)

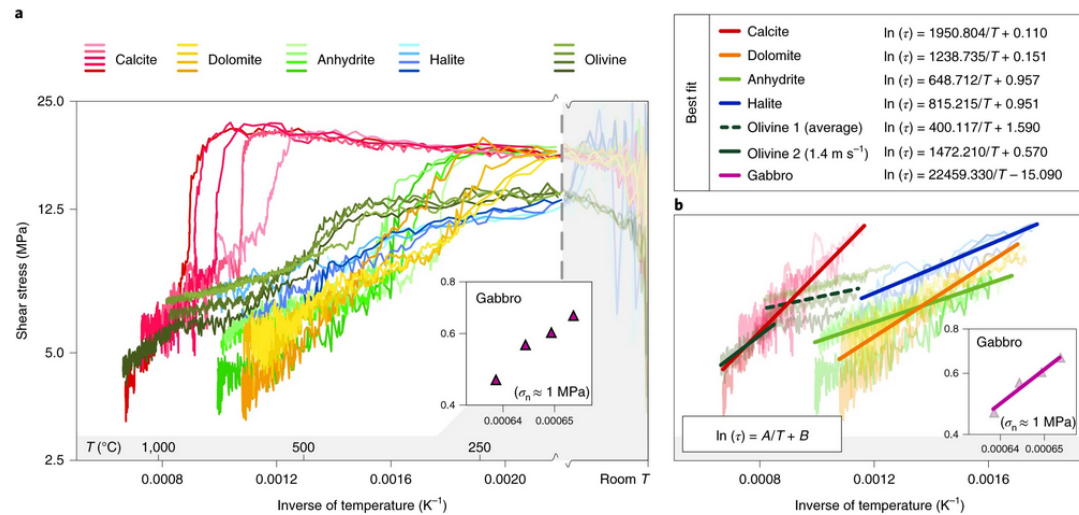
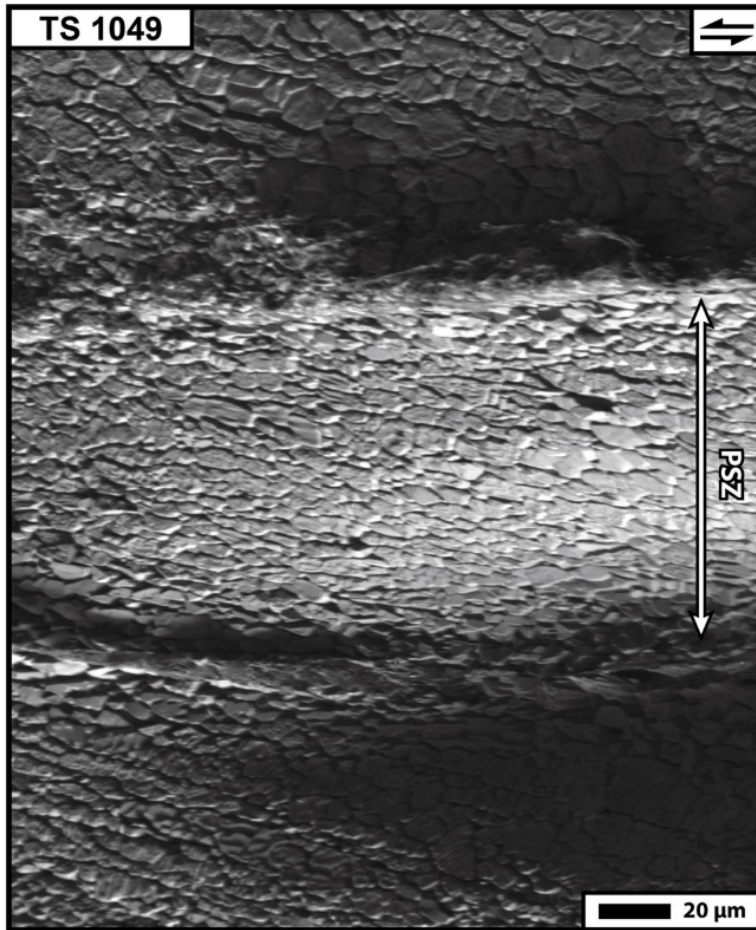


Figure 28: From (Pozzi, De Paola, Stefan Nielsen, et al. 2021)



In the previous section we have looked at evidence of crystal plasticity as a possible efficient mechanism for thermally-enhanced weakening. But temperature rise can trigger other processes that are susceptible to enhance the weakening (e.g., melt lubrication, fluid pressurization, flash weakening, or other types of flow like dislocation climb or glide, twinning).

Each thermally triggered process has a narrow temperature range at which the kinetics are exponentially accelerating and where it will become efficient. As one process is active, but temperature continues to rise under frictional work, another mechanism may kick-in that is more efficient and take over. However, change of phase triggered by the temperature rise are generally endothermal, therefore offering a thermal buffer that prevents the temperature rise.

The most efficient process will depend on the rock composition, too. Because calcite decarbonation takes place at relatively modest temperatures ($\approx 825^{\circ}\text{C}$), this phase transition introduces a thermal buffer that prevents reaching melting temperatures. However, when the calcite is fully decarbonated (and transformed into lime), the temperature is able to rise again **VIDEO**, until it may reach its combustion temperature (around 2500 C).

A number i of flow mechanisms could in principle be active in a latent state, however, only the most efficient one at the given temperature and grain size will be manifest:

$$\dot{\gamma}_{tot} = C_1 \tau^{n_1} e^{-\frac{H_1}{RT}} D^{m_1} + C_2 \tau^{n_2} e^{-\frac{H_2}{RT}} D^{m_2} + \dots + C_i \tau^{n_i} e^{-\frac{H_i}{RT}} D^{m_i} \quad (25)$$

Minerals from rocks of different composition (e.g. silicates such granite, basalt) do not have low decomposition temperature and are more likely to reach the melting temperature before another weakening process is triggered. In this case the flash weakening stage (localised melting of asperities) can be more or less rapidly followed by frictional melt, where a melt / clast suspension pervades the whole fault interstitial space allowing efficient melt lubrication.

Frictional melt

Frictional melt is an interesting earthquake fault process, if only because it is, to this day, the most unambiguous marker of seismic activity, and because it can be used as a gage for co-seismic frictional heating as originally proposed by

Sibson 1975. Although it is unclear how pervasive it is, the solidified product of frictional melt (rapidly solidified melt: pseudotachylite or PT) is observed on a number of exhumed natural fault outcrops.

For frictional in the presence of extrusion, one may use a modified diffusion equation with a transport term

$$\partial_t T = \kappa \partial_z^2 T + v \partial_z T + \frac{\delta(z) q}{\rho c}; \quad (26)$$

where v is the migration velocity of the melting boundary. This is known as a Stefan problem, and has a simple steady-state solution in the case of $v = const.$

The frictional melting with extrusion dynamics can be applied to faults where most melt is extruded to lateral veins. In this case, it can be shown (S. Nielsen, Toro, T. Hirose, et al. 2008) that the normal stress dependence of friction is a powerlaw in $\sigma_n^{1/4}$, it is a form of lubrication as at high normal stress, the dependence is much weaker than the linear trend of Byerlee's friction.

- PT as a marker of seismic dynamics and directivity
- PT as a gauge for sliding friction on seismic faults
- PT as a gauge of frictional power (and slip velocity) on seismic faults

(Fig. 30), (Fig. 31), (Fig. 32), (Fig. 33), (Fig. 34), (Fig. 36), (Fig. 37), (Fig. 38), (Fig. 39)

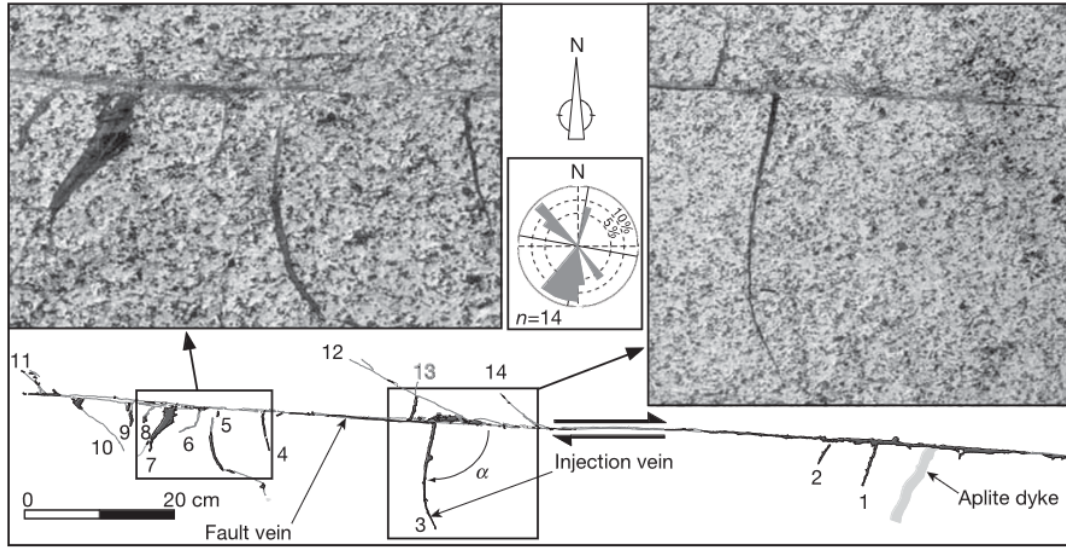
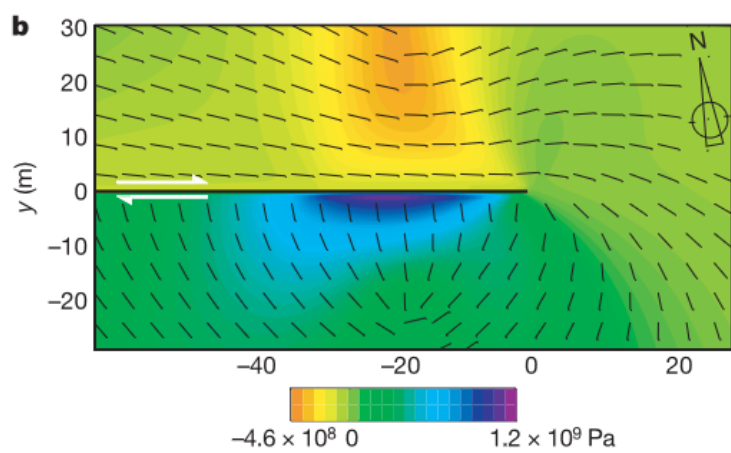
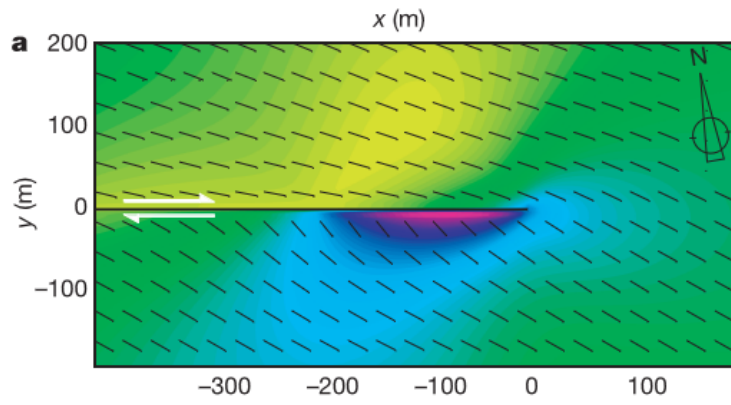


Figure 30:



c Large anelastic strain and plasticity



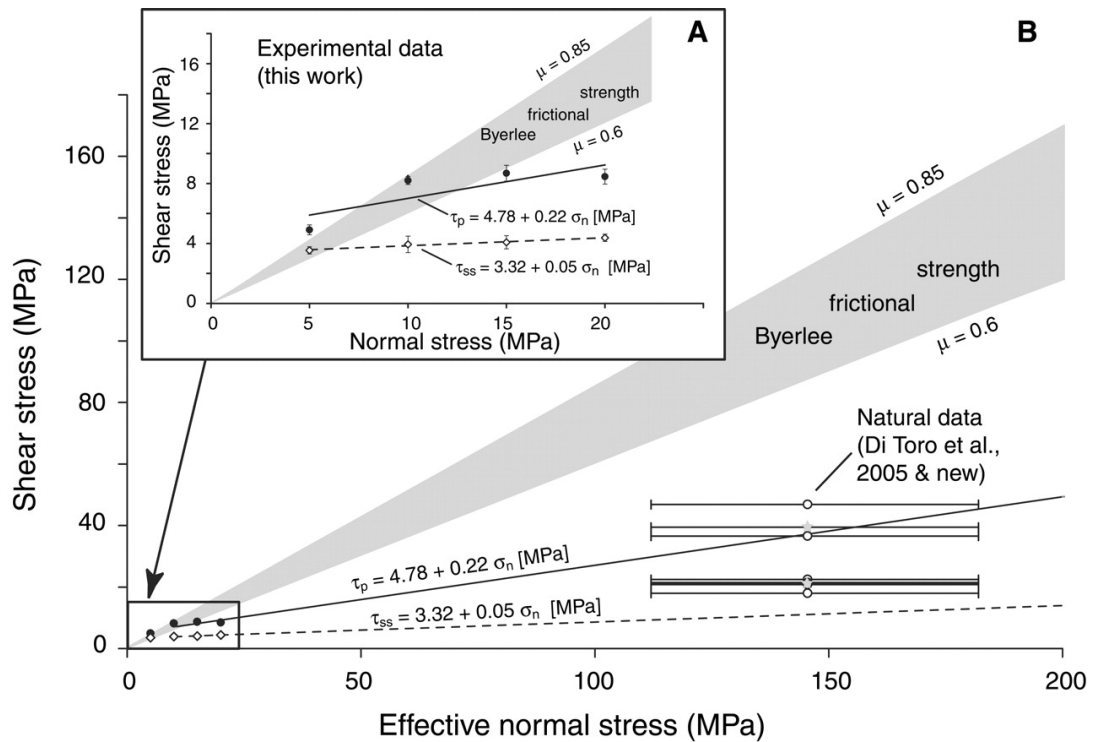


Figure 32: From (Giulio Di Toro, Takehiro Hirose, Stefan Nielsen, et al. 2006)

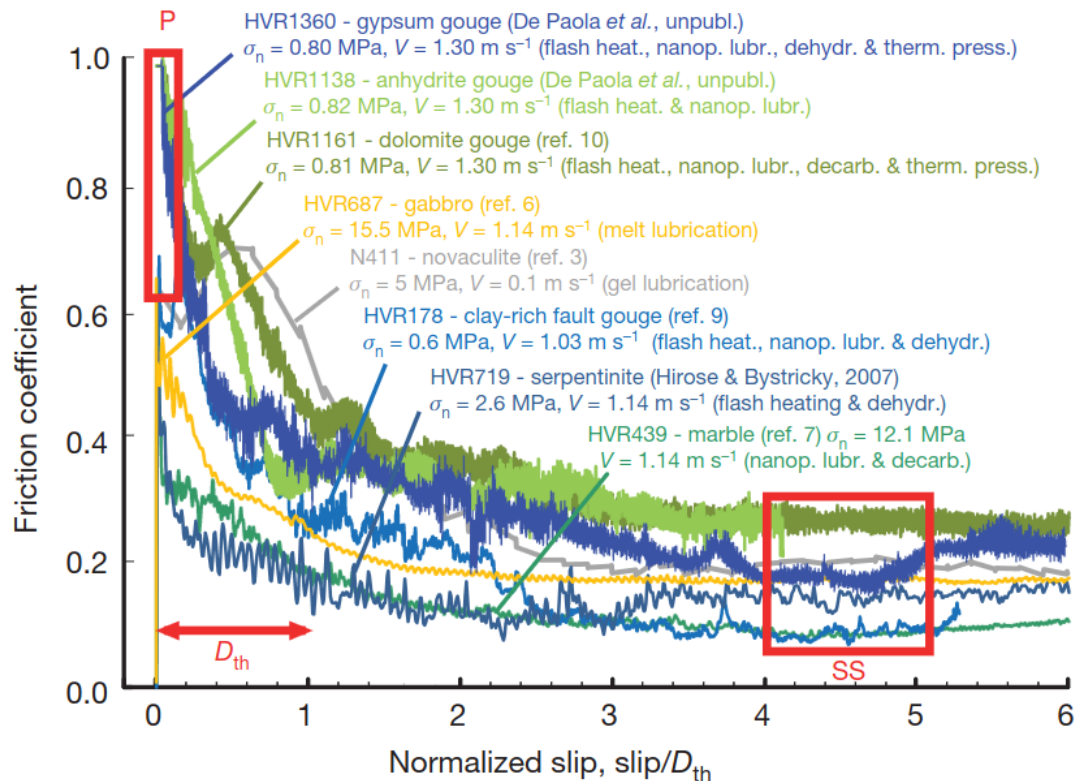


Figure 33: From (G. Di Toro, Han, T. Hirose, et al. 2011)

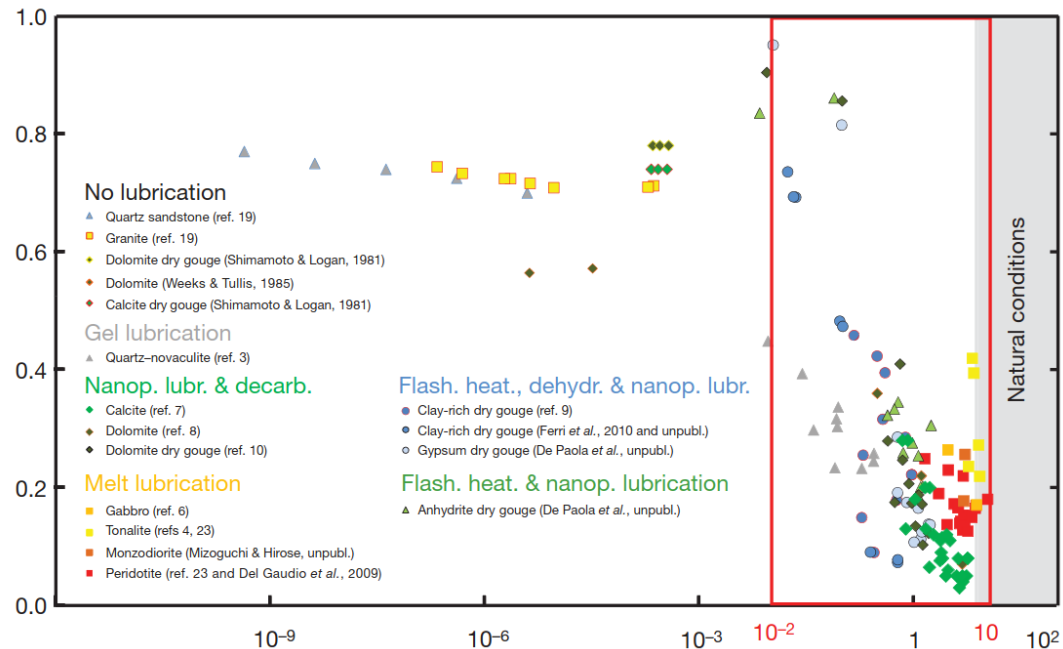


Figure 34: From (G. Di Toro, Han, T. Hirose, et al. 2011)

Thermal gradient and melt embayments

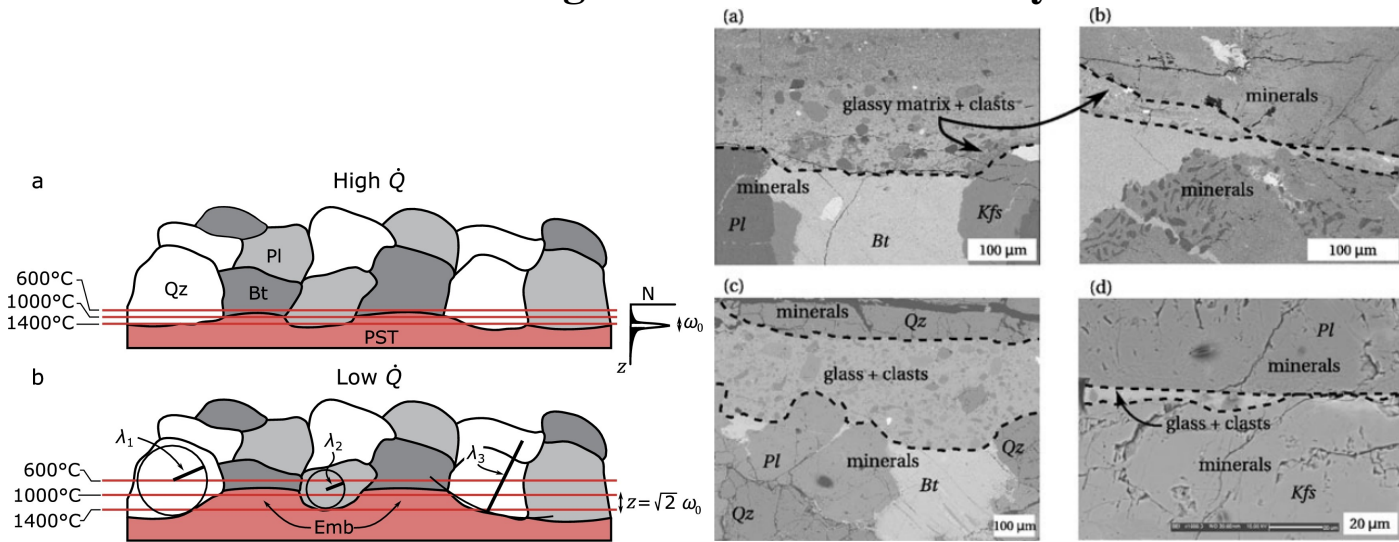


Figure 35: The thermal gradient introduces a difference in elevation (embayments) between low and high melting temperature minerals. A steeper gradient corresponding to a higher heat rate, and produces smaller embayments.

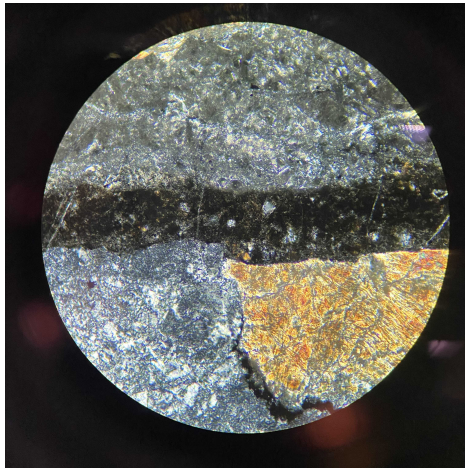


Figure 36: Peridotite (upper mantle) with PT and embayment. Field of view is ≈ 2 mm. Origin of the sample Balmuccia, Western Alps, Italy. Spinel has a lower melting temperature than Orthopyroxene by a few hundred degrees, which creates the embayment in the PT / mineral boundary on the bottom side of the fault vein.

In the field

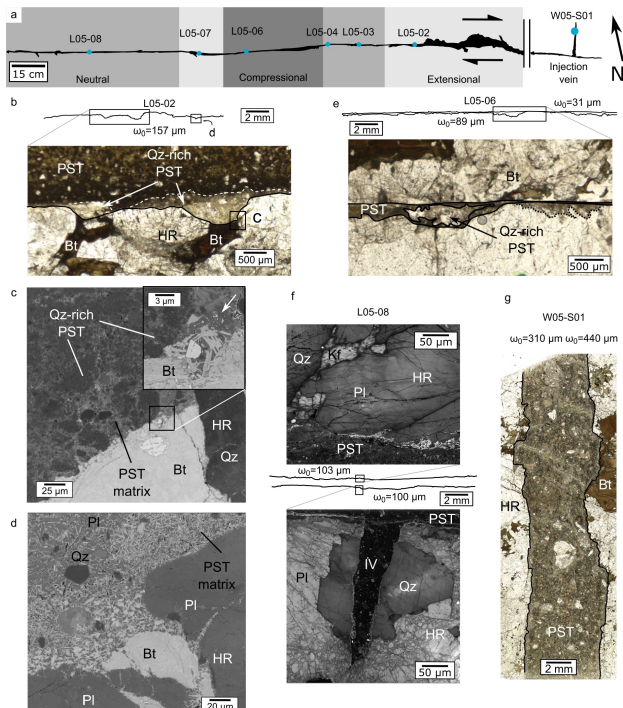


Figure 37: Fault vein and microstructures

In the Experiment

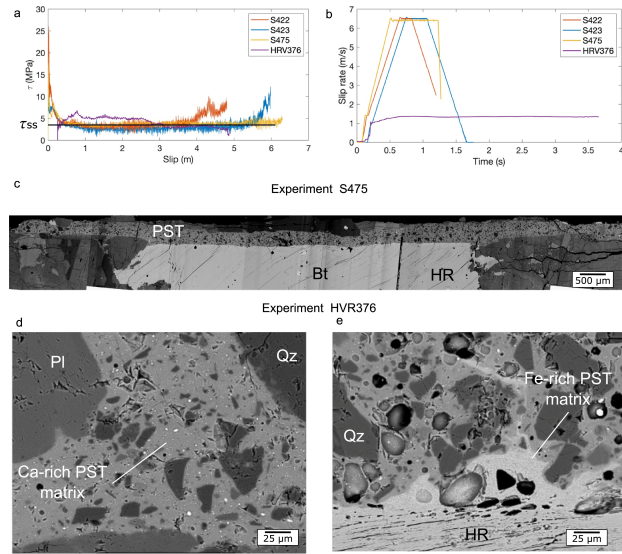


Figure 38: Experiment and PT micro-roughness. From Lazari, Castagna, S. Nielsen, et al. 2023

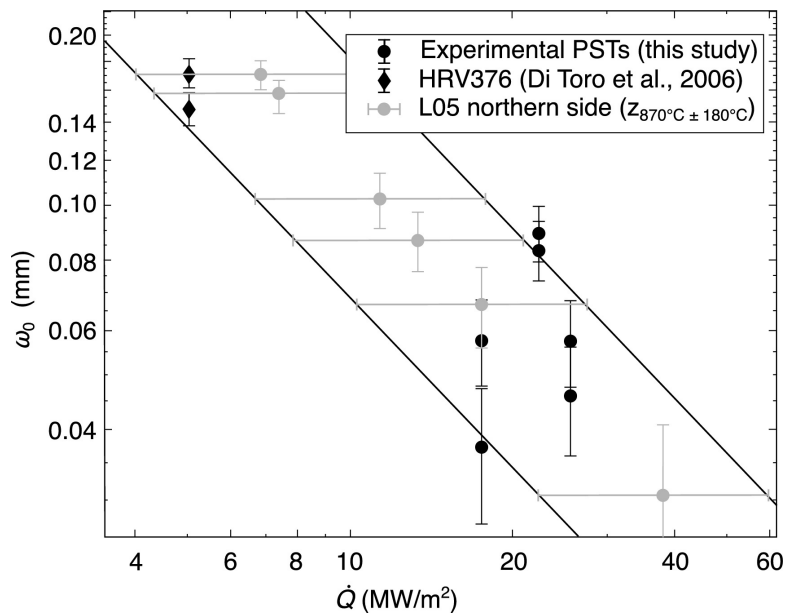


Figure 39: From(Lazari, Castagna, S. Nielsen, et al. 2023)

Exercise:

Find the steady state solution to 26 inside the solid, with $v = const.$ Hint: use T_m (melting temperature) as a boundary condition, no heat source (it's only inside the melt), and use a moving boundary attached to the solid/melt boundary. (To check your result, see solution

in S. Nielsen, Toro, T. Hirose, et al. 2008.

Fluid pressurization

- Buffering of flash weakening by fluids

Fluid pressurization is another mechanism that produces fault weakening as a consequence of frictional heating. The direct effect of pressure P_f is to relieve the effective normal stress by an amount αP where α is the Biot coefficient. α is poorly constrained and usually the limit value $\alpha = 1$ is assumed. The pressure increase is linked to the thermal expansion coefficient of the fluid (often brine or water) in a confined volume. Because friction is proportional to normal stress –save on lubricated interfaces– then the pressure results in a reduction of sliding frictional stress proportional to P_f :
$$\tau = \mu(\sigma_n - \alpha P_f)$$

However P_f is not directly proportional to T rise; indeed a change in the fault vein volume will take place in response to pressurization. In addition, the permeability of the host rock is an important parameter, and secondary fractures in the host rock will provide escape routes for the fluid, thus alleviating the pressure rise.

Recent experiments (Acosta, Passelègue, Schubnel, et al. 2018) suggest that flash heating and pressurization can compete with each other during seismic slip, and the dominant mechanism will depend on factors such as initial fluid pressure. At low (1 MPa) fluid pressure conditions or in dry conditions, flash weakening will dominate. Under higher fluid pressure (25 MPa), water's liquid-supercritical phase transition absorbs sufficient heat to buffer the temperature rise. This buffer effect is decreasing again at depths greater than a few kilometers.

(Fig. 40)

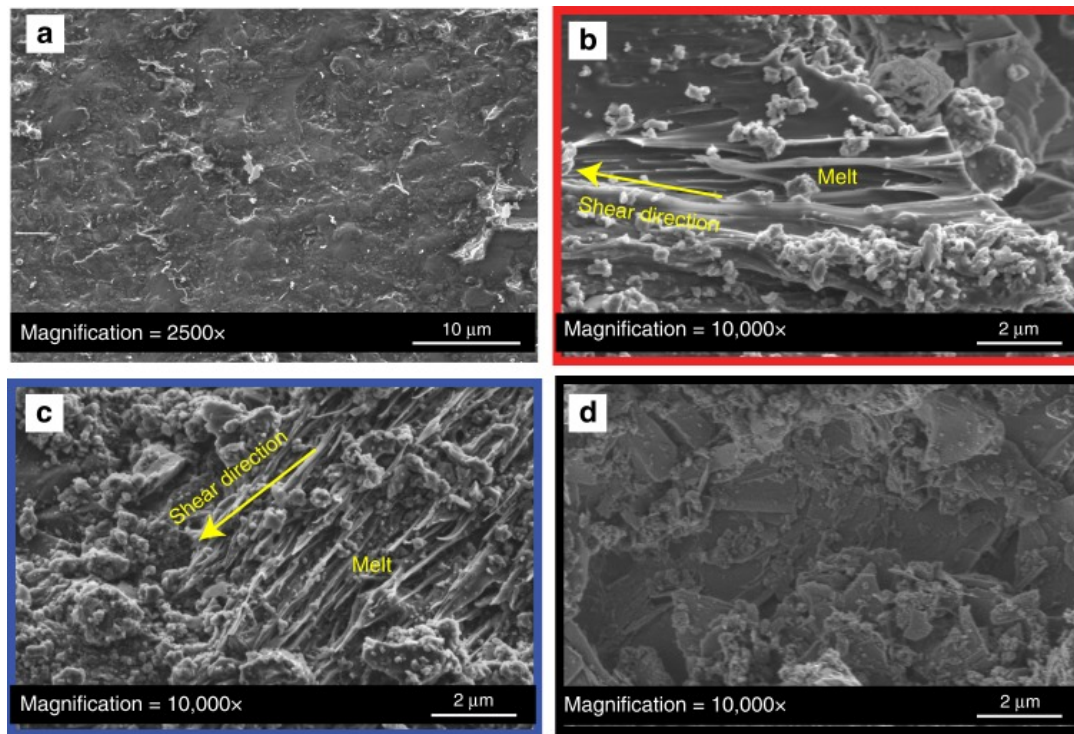


Figure 40:

The pressurization does not necessarily affect the fluid that is present in the rock from the outset, but also fluids that are the by-product of thermal decomposition. One example is the decarbonation of dolomite that is believed to have taken

place in the giant landslide of Heart Mountain (T. M. Mitchell, S. A. Smith, Anders, et al. 2015). The dolomite grains adjacent to the PSZ contain vesicular rims and planar trails of vesicles typical of decarbonation. An experimental analog was produced in the laboratory as shown in (Fig. 41)

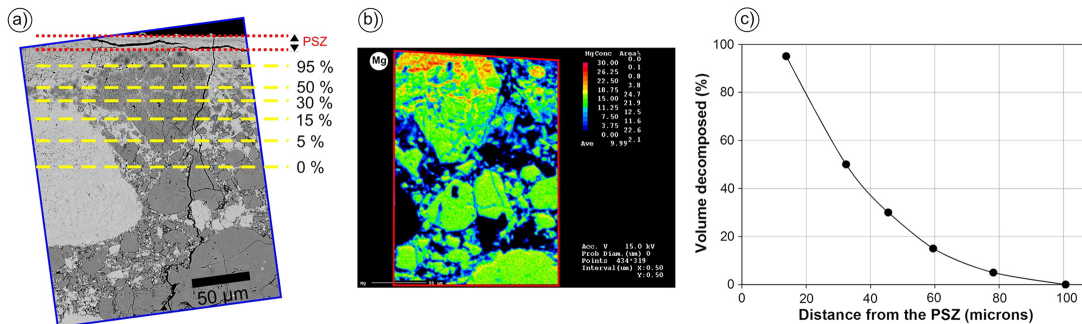


Figure 41:

Slip arrest and friction recovery

Rate-weakening and the healing effect, cracks and pulses, dynamic complexity, cf. Bruce Shaw!...

Practical projects –your choice!

- Evaluate friction from melt volume on fossil earthquake rocks. Is it very low, and why? Is it independent of slip, and why? If there is a slip dependence, what type of function appears to fit it best (use loglog maybe)? Is there a characteristic length?

To do this, use that shear stress times slip is work per unit fault area (N m^{-2}), and that melt volume is proportional to the amount of heat produced by frictional shear per unit fault area. You should use Table (1) and the following parameters: latent heat $L=400 \times 10^3 \text{ J kg}^{-1}$, mass density $\rho=2800 \text{ kg m}^{-3}$, heat capacity $C_p = 1200 \text{ J kg}^{-1} \text{ C}^{-1}$, clast fraction within melt $\phi = 0.05$, average melting temperature $T_m = 1300 \text{ C}$, depth = 8 km, vertical thermal gradient 25°C km^{-1} . Useful equations:

$$\tau \times U = w \times E \times \rho \quad (27)$$

$$E = L(1 - \phi) + C_p(T_m - T_i) \quad (28)$$

- Compute equivalent \mathbf{G}_c from friction experimental data. How does it compare to seismological estimates? Use the data from rotary shera experiments S324, S543 and S620 in files S0620_SlipStress.csv, slistre324.csv, slistre543.csv.
- Quantify dissipation in a distributed volume (multiple fault strands). Discuss your strategy to integrate this in the energy balance. How to integrate such a dissipation in fracture energy, or in friction, or both?

Use the table in file *fracture-energy_data.xlsx* that reports slip measured on each of the observed sub-faults. Use the linear slip-weakening approximation of figure (Fig. 42) with $\tau_p = 6 \text{ MPa}$, $\tau_r = 0.9 \text{ MPa}$, $D_w = 0.06 \text{ m}$ ($G_c = E_G$ is the blue area triangle).

Separation mm	Thickness mm	Separation mm	Thickness mm
7.0	0.5	75.0	1.4
3.4	0.2	43.0	0.4
28.0	1.3	65.0	0.3
18.0	0.5	57.0	0.6
67.0	1.5	420.0	3.1
88.0	1.8	630.0	2.8
82.0	1.5	480.0	1.9
71.0	1.3	78.0	1.6
58.0	1.0	49.0	0.4
117.0	2.0	94.0	1.3
68.0	0.8	82.0	0.7
243.0	2.3	150.0	1.8
1290.0	7.5	310.0	1.4
910.0	3.3	59.0	0.6
22.0	0.3	275.0	1.3
24.0	1.1	685.0	2.8
12.0	0.7	35.0	0.4
55.0	1.4	43.0	0.5
31.0	0.4	41.0	0.6
26.0	0.2	76.0	0.7
80.0	1.4	120.0	0.7
25.0	0.5	46.0	0.3
18.0	0.8	11.0	0.5
65.0	0.8	1670.0	1.8

Table 1: Data measured on pseudotachylite-bearing faults in the outer Hebrides. Separation is the apparent offset measured in the field across the fault; here we assume that separation equates to slip (i.e., that the outcrop surface was parallel to the slip direction). The thickness is an average (obtained by dividing the pseudotachylite area visible at the surface, by the fault length). Data from (S. Nielsen, Mosca, Giberti, et al. 2010; Sibson 1975). Depth at time of seismicity: 7-9 km.

4. Frictional heating: compute temperature, heat, and potential phase transitions at different slip rates. How early in the slip is the transition expected in real Earth conditions?
5. Compute frictional shear stress from plastic flow laws
6. Calculate rupture velocity on a simple mathematical fault, using a stress intensity K-integral
7. Calculate dynamic rupture with a prescribed friction law using a numerical modelling (finite differences, finite elements, code of Ampuero?). Compare to the K-integral.

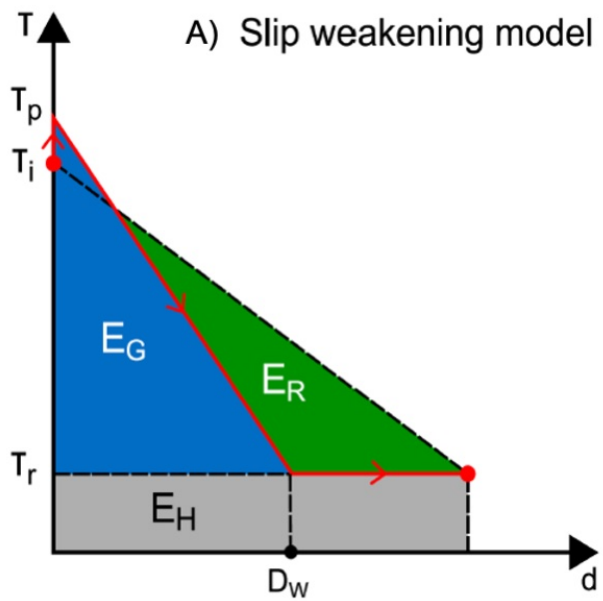


Figure 42:

Appendix I. Divergence theorem and energy

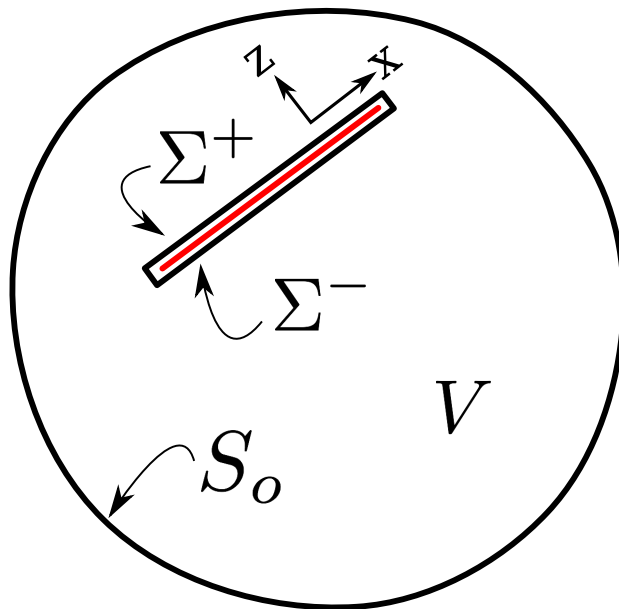


Figure 43: Schematic section of the Earth intersecting a fault surface (in red). The total Earth volume is V , S_o is the traction-free surface of the Earth, and the surface $\Sigma = \Sigma^+ + \Sigma^-$ snugly surrounds the fault. By making Σ^+ and Σ^- infinitesimally close, the volume between S and Σ can include all of V .

A full treatment of the energy change in earthquake can be found in Kostrov, Dhalen (...), which is here presented in a simplified fashion. First we state the divergence theorem. For a vector field \mathbf{F} in a volume V , enclosed within a surface S :

$$\iiint_V (\nabla \cdot \mathbf{F}) dV = \iint_S (\mathbf{F} \cdot \mathbf{n}) dS. \quad (29)$$

and its equivalent formulation applied to a tensor σ or σ_{ij} using Einstein notation (implicit summation on repeated indexes) for a tensor:

$$\iiint_V \partial_j (\sigma_{ij}) dV = \iint_S n_j \sigma_{ij} dS. \quad (30)$$

where n_i is the i_{th} component of the local normal vector \mathbf{n} pointing outwards from the surface S . Second, we recall the definition of strain energy density (p.u. volume) as the product of stress and strain, namely

$$\rho_{\text{strain}} = 1/2 \sigma_{ij} \epsilon_{ij} \quad (31)$$

(with implicit summation over all indexes i, j). The earthquake "driving energy" E originates in the release of stored elastic strain, which is converted to in forms, including frictional dissipation, creation of new fractures and radiation of kinetic energy (waves). The difference between the stored strain energy *before* and *after* the rupture, in terms of local density, can be written as:

$$\rho_E = 1/2 (\sigma_{ij}^1 \epsilon_{ij}^1 - \sigma_{ij}^0 \epsilon_{ij}^0) \quad (32)$$

where the superscripts 1 and 0 refer to the final and initial conditions, respectively. Then the total strain energy change E_{tot} can be obtained by integrating in the volume V surrounding the fault:

$$E_{tot} = 1/2 \iiint_V (\sigma_{ij}^1 \epsilon_{ij}^1 - \sigma_{ij}^0 \epsilon_{ij}^0) dV \quad (33)$$

From ρ_w of eq. (32) let's try to get an expression based only on initial stress σ_{ij}^0 , stress difference $\Delta\sigma_{ij} = \sigma_{ij}^1 - \sigma_{ij}^0$ and strain difference $\Delta\varepsilon_{ij} = \varepsilon_{ij}^1 - \varepsilon_{ij}^0$:

$$\begin{aligned}\rho_E &= 1/2 (\sigma_{ij}^0 + \Delta\sigma_{ij}) (\varepsilon_{ij}^0 + \Delta\varepsilon_{ij}) - 1/2 \sigma_{ij}^0 \varepsilon_{ij}^0 \\ &= 1/2 (\sigma_{ij}^0 \Delta\varepsilon_{ij} + \Delta\sigma_{ij} \varepsilon_{ij}^0 + \Delta\sigma_{ij} \Delta\varepsilon_{ij})\end{aligned}\quad (34)$$

To further simplify the expression, we can assume purely elastic strain in the volume surrounding the fault, with a constitutive law (Hooke's law) relating stress term to strain via the linear elasticity.

Take good note here that we apply the divergence theorem only to the elastic part of the deformation. Therefore, we will need to exclude form this energy change using the divergence theorem, all volumes of rock where nonlinear or anelastic processes take place, and treat those separately. In particular, volumes within which plastic deformation or frictional dissipative processes take place will be excluded. In this specific treatment, we will assume that they take place within a volume of infinitesimal thickness –a mathematical fault surface.

For convenience we may use the elastic modulus tensor c_{ijkl} such that:

$$c_{ijkl} = \lambda \delta_{ij} \delta_{kl} + G (\delta_{ik} \delta_{jl} + \delta_{il} \delta_{jk}) \quad (35)$$

and then write the stress-strain Hooke's law as:

$$\begin{aligned}\sigma_{ij} &= c_{ijkl} \varepsilon_{kl} \\ \Delta\sigma_{ij} &= c_{ijkl} \Delta\varepsilon_{kl} \\ \varepsilon_{ij}^0 &= \frac{\sigma_{kl}^0}{c_{kl} c_{ij}}\end{aligned}\quad (36)$$

therefore

$$\begin{aligned}
 \rho_E &= 1/2 (\sigma_{ij}^0 + \Delta\sigma_{ij}) (\epsilon_{ij}^0 + \Delta\epsilon_{ij}) - 1/2 \sigma_{ij}^0 \epsilon_{ij}^0 \\
 &= 1/2 \left(\sigma_{ij}^0 \Delta\epsilon_{ij} + \cancel{c_{ijkl}} \Delta\epsilon_{kl} \frac{\sigma_{kl}^0}{\cancel{c_{kl}} \cancel{j}} + \Delta\sigma_{ij} \Delta\epsilon_{ij} \right) \\
 &= 1/2 (\sigma_{ij}^0 \Delta\epsilon_{ij} + \Delta\epsilon_{kl} \sigma_{kl}^0 + \Delta\sigma_{ij} \Delta\epsilon_{ij})
 \end{aligned} \tag{37}$$

where the symmetry property $c_{ijkl} = c_{kl}ij$ has been used to eliminate the elastic moduli. Because of the implicit summation all repeated indexes are dummies so we know that $\Delta\epsilon_{kl} \sigma_{kl}^0 = \Delta\epsilon_{ij} \sigma_{ij}^0$ and therefore after replacing the $\Delta\sigma_{ij}$ we obtain:

$$\rho_E = 1/2 \Delta\epsilon_{ij} (\sigma_{ij}^0 + \sigma_{ij}^1) \tag{38}$$

The total energy change is obtained by integrating the density on all the volume

$$E_{tot} = 1/2 \iiint_V \Delta\epsilon_{ij} (\sigma_{ij}^0 + \sigma_{ij}^1) dV \tag{39}$$

Furthermore we have that

$$\begin{aligned}
 \partial_i (\sigma_{ij} u_j) &= \cancel{\partial_i (\sigma_{ij})} u_j + \sigma_{ij} \partial_i (u_j) \\
 &= \sigma_{ij} \partial_i (u_j)
 \end{aligned} \tag{40}$$

because at equilibrium $\partial_i (\sigma_{ij}) = 0$. If u_i is the displacement of particles between before and after the rupture, by definition of the infinitesimal strain we have

$$\Delta\epsilon_{ij} = 1/2 (\partial_i u_j + \partial_j u_i) \tag{41}$$

and because of the summation on all indexes we are allowed to write:

$$\sigma_{ij} \Delta\epsilon_{ij} = \sigma_{ij} \partial_i u_j = \partial_i (\sigma_{ij} u_j) \tag{42}$$

Finally we can re-write the volume integral of W such that:

$$E_{tot} = 1/2 \iiint_V \partial_i [(\sigma_{ij}^0 + \sigma_{ij}^1) u_j] dV \quad (43)$$

We may now apply the divergence theorem to write:

$$E_{tot} = 1/2 \iiint_V \partial_i [(\sigma_{ij}^0 + \sigma_{ij}^1) u_j] dV = 1/2 \iint_S n_i (\sigma_{ij}^0 + \sigma_{ij}^1) u_j dS \quad (44)$$

We may split S into two parts $S = S_o + \Sigma$ (Fig. 43). Σ is a surface snugly fitted around the fault, and S_o is the free surface of the Earth. Now because the free traction condition on the surface S_o is $\mathbf{T}(\mathbf{n}) = 0$ where \mathbf{T} is traction; traction and stress are related by $T_j = \sigma_{ji} n_i$. Therefore the integral over S_o will vanish at any time, and we're left with

$$E_{tot} = 1/2 \iint_{\Sigma} n_i (\sigma_{ij}^0 + \sigma_{ij}^1) u_j d\Sigma \quad (45)$$

So we have been able to show that the total energy change can be represented by a surface which can be made arbitrarily close to the fault surface, until we are for all practical purposes describing values of σ_{ij} and u_i which are effectively *on* the fault surface. To further simplify the expression, we can use a geometry where the fault normal is z , the fault is located along (x,y) plane at $z = 0$ and the slip occurs in direction x (Fig. 43). In this case the fault normal vector is $\mathbf{n} = (n_x, n_y, n_z) = (0, 0, 1)$, slip motion on the fault is $\mathbf{u} = (u_x, 0, 0)$ and

$$E_{tot} = 1/2 \iint_{\Sigma} (\sigma_{zx}^0 + \sigma_{zx}^1) u_x d\Sigma \quad (46)$$

Letting Σ^- be adjacent to the "bottom" part of the fault ($z \rightarrow 0^-$) and Σ^+ be adjacent to the "top" part of the fault ($z \rightarrow 0^+$), defining slip $D = u_x^+ - u_x^-$, and using traction continuity such that $\sigma_{xz}^+ = \sigma_{xz}^-$ and symmetry ($\sigma_{zx} = \sigma_{xz}$) we can write

$$\begin{aligned} E_{tot} &= 1/2 \iint_{\Sigma^+} (\sigma_{xz}^0 + \sigma_{xz}^1) u_x d\Sigma - 1/2 \iint_{\Sigma^-} (\sigma_{xz}^0 + \sigma_{xz}^1) u_x d\Sigma \\ &= 1/2 \iint_{\Sigma} (\sigma_{xz}^0 + \sigma_{xz}^1) D d\Sigma \end{aligned} \quad (47)$$

and taking average values for stress and slip on the fault, and defining $\sigma = \sigma_{xz}$ where the subscripts are implicit we can write:

$$\begin{aligned} E_{tot} &= 1/2 \iint_{\Sigma} (\sigma_{xz}^0 + \sigma_{xz}^1) D d\Sigma \\ &= \frac{\overline{\sigma^0 + \sigma^1}}{2} \overline{D} \iint_{\Sigma} d\Sigma \\ E_{tot} &= \frac{\overline{\sigma^0 + \sigma^1}}{2} \overline{D} \Sigma \end{aligned} \quad (48)$$

Expression (48) shows that the total energy change in the volume can be calculated from the initial and final stress defined on the fault surface Σ alone. The only net work applied to the Earth-system during the earthquake is the result of the stress change on the fault surface (provided that all nonlinear processes are confined onto the surface).

References

- Abercrombie, Rachel E. and James R. Rice (Aug. 2005). “Can observations of earthquake scaling constrain slip weakening?” In: *Geophysical Journal International* 162.2, pp. 406–424. DOI: 10.1111/j.1365-246x.2005.02579.x.
- Acosta, M. et al. (2018). “Dynamic weakening during earthquakes controlled by fluid thermodynamics”. In: *Nature Communications* 9.1. DOI: 10.1038/s41467-018-05603-9.
- Aki, K and P. Richards (2002). *Quantitative Seismology, second edition*. Science University Books.
- Aldrighetti, Silvia (2023). “Estimate of seismic surface energy from microstructural studies of pseudotachylite-bearing faults”. In: *TESI DI LAUREA MAGISTRALE IN GEOLOGIA AMBIENTALE E DINAMICA DELLA TERRA, Universita di Padova*.
- Archard, J.F. (1959). “The temperature of rubbing surfaces”. In: *Wear* 2.6, pp. 438–455. ISSN: 0043-1648. DOI: 10.1016/0043-1648(59)90159-0.
- Broberg, K. B. (1999). *Cracks and Fracture*. Academic Press. ISBN: 9780121341305.
- Brown, Stephen R. and Christopher H. Scholz (June 1985). “Closure of random elastic surfaces in contact”. In: *Journal of Geophysical Research: Solid Earth* 90.B7, pp. 5531–5545. DOI: 10.1029/jb090ib07p05531.
- Candela, Thibault et al. (Aug. 2012). “Roughness of fault surfaces over nine decades of length scales”. In: *Journal of Geophysical Research: Solid Earth* 117.B8, n/a–n/a. DOI: 10.1029/2011jb009041.
- Carslaw, H. S. and J. C. Jaeger (1990). *Conduction of Heat in Solids*. Oxford University Press, USA.
- Cocco, Massimo et al. (2023). “Fracture Energy and Breakdown Work During Earthquakes”. In: *Annual Review of Earth and Planetary Sciences* 51.1, pp. 217–252. DOI: 10.1146/annurev-earth-071822-100304.
- Davies, J. H. and D. R. Davies (Feb. 2010). “Earth’s surface heat flux”. English. In: *Solid Earth* 1.1. Publisher: Copernicus GmbH, pp. 5–24. ISSN: 1869-9510. DOI: 10.5194/se-1-5-2010. (Visited on 09/27/2023).
- Di Toro, G. et al. (Mar. 2011). “Fault lubrication during earthquakes”. In: *Nature* 471.7339, pp. 494–498. DOI: 10.1038/nature09838.

- Di Toro, Giulio, Stefan Nielsen, and Giorgio Pennacchioni (Aug. 2005). "Earthquake rupture dynamics frozen in exhumed ancient faults". In: *Nature* 436.7053, pp. 1009–1012. DOI: 10.1038/nature03910.
- Di Toro, Giulio et al. (Feb. 2006). "Natural and Experimental Evidence of Melt Lubrication of Faults During Earthquakes". In: *Science* 311.5761, pp. 647–649. DOI: 10.1126/science.1121012.
- Dieterich, James H. and Brian D. Kilgore (May 1996). "Imaging surface contacts: power law contact distributions and contact stresses in quartz, calcite, glass and acrylic plastic". In: *Tectonophysics* 256.1-4, pp. 219–239. DOI: 10.1016/0040-1951(95)00165-4.
- Fossum, A. F. and L. B. Freund (Aug. 1975). "Nonuniformly moving shear crack model of a shallow focus earthquake mechanism". In: *Journal of Geophysical Research* 80.23, pp. 3343–3347. DOI: 10.1029/jb080i023p03343.
- Goldsby, D. L. and T. E. Tullis (Oct. 2011). "Flash Heating Leads to Low Frictional Strength of Crustal Rocks at Earthquake Slip Rates". In: *Science* 334.6053, pp. 216–218. ISSN: 1095-9203. DOI: 10.1126/science.1207902.
- Greenwood, J. A. and J. B. P. Williamson (1966). "Contact of nominally flat surfaces". In: *Proceedings of the Royal Society of London. Series A, Mathematical and Physical Sciences* 295.1442, pp. 300–319.
- Kanamori, Hiroo and Luis Rivera (2006). "Energy partitioning during an earthquake". In: *Earthquakes: Radiated Energy and the Physics of Faulting*. American Geophysical Union, pp. 3–13. DOI: 10.1029/170gm03.
- Lazari, F. et al. (2023). "Frictional power dissipation in a seismic ancient fault". In: *Earth and Planetary Science Letters* 607, p. 118057. DOI: 10.1016/j.epsl.2023.118057.
- Madariaga, Raul (May 2007). "Slippery When Hot". In: *Science* 316.5826, pp. 842–843. DOI: 10.1126/science.1142332.
- Mitchell, T.M. and D.R. Faulkner (Aug. 2009). "The nature and origin of off-fault damage surrounding strike-slip fault zones with a wide range of displacements: A field study from the Atacama fault system, northern Chile". In: *Journal of Structural Geology* 31.8, pp. 802–816. DOI: 10.1016/j.jsg.2009.05.002.

- Mitchell, Thomas M. et al. (Feb. 2015). "Catastrophic emplacement of giant landslides aided by thermal decomposition: Heart Mountain, Wyoming". In: *Earth and Planetary Science Letters* 411, pp. 199–207. DOI: 10.1016/j.epsl.2014.10.051.
- Nielsen, S., G. di Toro, and W. A. Griffith (2010). "Friction and roughness of a melting rock surface". In: *Geophysical Journal International*. DOI: 10.1111/j.1365-246x.2010.04607.x.
- Nielsen, S., E. Spagnuolo, M. Violay, and G. Di Toro (2021). "Thermal Weakening Friction During Seismic Slip: Experiments and Models With Heat Sources and Sinks". In: *Journal of Geophysical Research: Solid Earth* 126.5. DOI: 10.1029/2020jb020652.
- Nielsen, S., E. Spagnuolo, M. Violay, S. Smith, et al. (Mar. 2016). "G: Fracture energy, friction and dissipation in earthquakes". In: *Journal of Seismology* 20.4, pp. 1187–1205. DOI: 10.1007/s10950-016-9560-1.
- Nielsen, S. et al. (Jan. 2008). "Frictional melt and seismic slip". In: *Journal of Geophysical Research: Solid Earth* 113.B1. DOI: 10.1029/2007jb005122.
- Nielsen, S. et al. (2010). "On the transient behavior of frictional melt during seismic slip". In: *Journal of Geophysical Research: Solid Earth* 115.B10. DOI: <https://doi.org/10.1029/2009JB007020>.
- Nielsen, S. et al. (2016). "Scaling in natural and laboratory earthquakes". In: *Geophysical Research Letters* 43.4. 2015GL067490, pp. 1504–1510. ISSN: 1944-8007. DOI: 10.1002/2015GL067490.
- Pacheco, Javier F. and Lynn R. Sykes (June 1992). "Seismic moment catalog of large shallow earthquakes, 1900 to 1989". In: *Bulletin of the Seismological Society of America* 82.3, pp. 1306–1349. ISSN: 0037-1106. DOI: 10.1785/BSSA0820031306.
- Persson, B. (2000). *Sliding Friction, Physical Principles and Applications*. Springer-Verlag, New York.
- Pozzi, Giacomo et al. (2021). "Coseismic fault lubrication by viscous deformation". In: *Nature Geoscience* 14, pp. 437–442. ISSN: 1752-0894. DOI: 10.1038/s41561-021-00747-8.

- Reches, Zeev, Xiaofeng Chen, and Brett Carpenter (2019). “Asperity failure control of stick-slip along brittle faults”. In: *ESSOAR*. DOI: 10.1002/essoar.10501044.1.
- Rice, J. R. (2006). “Heating and weakening of faults during earthquake slip”. In: *J. Geophys. Res.* 111, B05311. DOI: 10.1029/2005JB004006.
- Freund, L. B. (1990). *Dynamic fracture mechanics*. Cambridge University Press.
- Sibson, Richard H. (1975). “Generation of Pseudotachylite by Ancient Seismic Faulting”. In: *Geophysical Journal of the Royal Astronomical Society* 43.3, pp. 775–794. DOI: <https://doi.org/10.1111/j.1365-246X.1975.tb06195.x>.
- Spagnuolo, E. et al. (Apr. 2016). “An empirically based steady state friction law and implications for fault stability”. In: *Geophysical Research Letters* 43.7, pp. 3263–3271. DOI: 10.1002/2016gl067881.
- Stern, Robert J. (2002). “Subduction Zones”. en. In: *Reviews of Geophysics* 40.4, pp. 3–1–3–38. ISSN: 1944-9208. DOI: 10.1029/2001RG000108.
- Violay, M. et al. (2015). “Thermo-mechanical pressurization of experimental faults in cohesive rocks during seismic slip”. In: *Earth Planet. Sci. Lett.* 429, pp. 1–10. ISSN: 0012-821X. DOI: 10.1016/j.epsl.2015.07.054.
- Xu, Shiqing et al. (Sept. 2014). “Dynamic Ruptures on a Frictional Interface with Off-Fault Brittle Damage: Feedback Mechanisms and Effects on Slip and Near-Fault Motion”. In: *Pure and Applied Geophysics* 172.5, pp. 1243–1267. DOI: 10.1007/s00024-014-0923-7.